Synthesis, Characterization and Electrochemical Hydrogen Insertion in ATP Capped Palladium Nanoparticles

by

Timothy Lamb

A Thesis Presented in Partial Fulfillment
of the Requirements for the Degree
Master of Science

Approved November 2013 by the
Graduate Supervisory Committee:

Daniel Buttry, Chair
Jeffery Yarger
Alexandra Ros

ARIZONA STATE UNIVERSITY

December 2013

ABSTRACT

Water-soluble, adenosine triphosphate (ATP)-stabilized palladium nanoparticles have been synthesized by reduction of palladium salt in the presence of excess ATP. They have been characterized by electron microscopy, energy dispersive X-ray spectroscopy, ultraviolet-visible (UV-Vis) spectroscopy, and X-ray diffraction in order to determine particle size, shape, composition and crystal structure. The particles were then subsequently attached to a glassy carbon electrode (GCE) in order to explore their electrochemical properties with regard to hydrogen insertion in 1 M sodium hydroxide. The particles were found to be in the size range 2.5 to 4 nm with good size dispersion. The ATP capping ligand allowed the particles to be air-stable and re-dissolved without agglomeration. It was found that the NPs could be firmly attached to the working electrode via cycling the voltage repeatedly in a NP/phosphate solution. Further electrochemical experiments were conducted to investigate the adsorption and absorption of hydrogen in the NPs in 1 M sodium hydroxide. Results for cyclic voltammetry experiments were consistent with those for nanostructured and thin-film palladium in basic solution. Absorbed hydrogen content was analyzed as a function of potential. The maximum hydrogen:Pd ratio was found to be ~0.7, close the theoretical maximum value for β phase palladium hydride.

DEDICATION

This is dedicated to my family for all of their love and support.

ACKNOWLEDGMENTS

I would like to acknowledge my amazing and supportive advisor, Prof. Buttry, whose brilliant insight helped tremendously in guiding my work. I am very grateful for thoughtful and patient encouragement and support. I'd also like to thank Prof. Yarger and Prof. Ros for their support and the Department of Chemistry at ASU where I discovered my passion for educating others.

I'd also like to thank the other members of my group for collaborating with each other to solve any problems. I'd like to thank members such as Harish, Poonam, Rajeev, Chris, Ashok, Tylan, Jarred, Russ, Kate, and Samrat for their valuable advice and support. Without thoughtful and insightful discussions with them, this would not be possible.

TABLE OF CONTENTS

Page

LIST OF TABLES

Table Page

LIST OF FIGURES

Figure Page

Chapter 1

GENERAL INTRODUCTION

Interest in nano-sized materials, especially nanoparticles (NPs) has increased dramatically in the past few decades. NPs are clusters of atoms of one or more elements having a diameter of less than 100 nanometers, which exhibit different properties than their bulk counterparts due to a much higher surface to volume ratio and electronic confinement[1]. Chemical properties such as catalytic behavior, and physical properties such as magnetism,[2,3] melting point,[1] and optical characteristics are different on the nanoscale compared to bulk. For example, gold colloids have been used as colorants in window glass due to their unique optical properties, allowing the NPs to absorb light of different wavelengths depending on their size.[4]

A unique feature of NPs is their larger surface to volume ratio. This leads to a variety of different effects that stem from the unusual properties of surface atoms. For example, surface atoms have a lower coordination number leading to a decreased stability compared to interior atoms. The relative surface area increases greatly as diameter decreases. Since only surface atoms are involved in catalysis, catalytic activity per unit mass also increases with decreasing diameter. This has driven considerable interest in characterization of the surfaces of NPs, especially with regard to chemisorption, a key step in catalysis.

Metal NPs are energetically very different from bulk samples. Metals such as gold, which are normally not very active can become effective catalysts at the nanoscale. For example, a reaction of great importance in all types of fuel cells is the reduction of oxygen, which is most commonly catalyzed by platinum.[5-7] Due to the high cost of

platinum, alternative catalysts are being investigated for this reaction such as gold,[8-11] silver,[12] and palladium.[13] Pd is also of interest because of its catalytic reactivity for hydrogen oxidation. This reaction is mediated through adsorbed H species. As will be seen below, H chemisorption on Pd NPs can be studied through their immobilization at carbon electrodes.

General Synthetic Methods

Because many NP properties depend strongly on size, much emphasis has been placed on synthesizing NPs with controllable size with low size dispersity, in order to precisely tune the NP properties. Low size dispersity is desirable because it facilitates the study of the size dependence of the NP properties. Efforts have also been made to synthesize metallic NPs with different shapes, utilizing the tendency of certain capping ligands to selectively arrest the growth of particular crystallographic planes and allow the growth of others.[14,15] An ideal synthetic method produces NPs with a uniform and highly controllable size and shape, with the final product able to be isolated and stored as a solid which can be later re-dissolved without aggregation or further growth. Common synthetic methods involve a bottom-up approach in which a metal salt is reduced in the presence of a stabilizing ligand, although other methods have been explored and will be discussed below.

Several mechanisms have been proposed for the formation of metal NPs. In the classical nucleation and growth mechanism, the LaMer mechanism, metal precursors are decomposed or reduced to metal atoms which then begin to aggregate into small metal clusters when a saturation of metal atoms is reached. Once the metal atom concentration falls below the saturation level, nucleation ceases while particles continue to grow via

atomic addition until an equilibrium is reached between solvated metal atoms and the NPs.[16] Metal NPs can also grow via Ostwald ripening in which smaller clusters are sacrificed to contribute to the growth of larger ones.[17,18] A mechanism proposed by Richards and co-workers is thought to involve formation of metal atoms via reduction, followed by the nucleation into small clusters, possible aggregation of clusters, and ultimate growth into NPs.[19] Indeed, it is believed that there is significant contribution to NP growth via this aggregation of clusters.[20] In some cases, the aggregation of clusters during growth can lead to polycrystalline NPs that contain domain boundaries. Chapter 2 shows an example of this for Pd NPs grown via tetrachloropalladate reduction with borohydride.

Many different sets of conditions have been used to produce metal NPs. As an example, a popular synthetic route developed by Brust et. al. for gold monolayer protected clusters (MPCs) is a two-phase synthesis in which tetrachloroaurate is dissolved in water and transferred to an organic phase (toluene) using tetraoctylammonium bromide (TOABr). The gold is then reduced with sodium borohydride in the organic phase in the presence of alkanethiolates, which bond to the surface of the gold and prevent further growth.[21] This method has been used to produce MPCs of silver,[22] palladium,[23,24] and other single metals and alloys. Single-phase synthesis methods are also routinely employed, as described in Chapter 2.

The function of the capping ligand is to arrest growth at a desired size and prevent aggregation and re-oxidation of metallic NPs. Some typical capping ligands used are alkanethiols as in the Brust synthesis[21] mentioned above, citrate,[25-27] and polymers such as polyvinylpyrrolidone (PVP).[28-31] Typically, the final size and dispersity of NPs can be

controlled primarily by changing the molar ratios of the capping ligand to the metal as well as the strength of the reducing agent with a higher proportion of capping ligand and a stronger reducing agent generally leading to smaller and more monodisperse NPs. An important function of the capping ligand is to control the solubility of the NPs after they have been formed. While there are many examples of hydrophobic capping ligands that endow NPs with solubility in non-aqueous solvents, as seen below, there are fewer examples of capping ligands that provide water soluble NPs. As will be seen in Chapter 2, we have developed a synthetic route to water soluble Pd NPs that allows the NP electrochemical behavior to be explored under aqueous conditions, an experimentally attractive condition. We also take advantage of an electrochemical process that drives release of the capping ligands, allowing the NPs to be facilely attached at electrode surfaces for electrochemical examination.

Characterization

Several characterization techniques are commonly utilized to determine NP size, shape, crystal structure, composition and electrochemical properties. Methods include atomic force microscopy (AFM), ultraviolet-visible spectroscopy (UV-Vis),[4,32] transmission electron microscopy (TEM) and high-resolution TEM (HRTEM), scanning electron microscopy (SEM) with energy dispersive x-ray spectroscopy (EDS), powder x-ray diffraction (XRD),[33] and infrared spectroscopy (IR).

AFM can be used to determine NP size. This method is also especially useful for determining the structure of assemblies of NPs. Many metallic and semiconductor NPs exhibit surface plasmon resonance (SPR) bands when interacting with ultraviolet or visible radiation.[4,32] UV-Vis spectroscopy can be used to characterize these spectral

features. Metals such as gold and silver show well-defined SPR peaks in the visible region.[34-36] The SPR peak shifts to the blue or red for smaller or larger NPs, respectively, and can therefore be used to aid in determination of NP size or to monitor growth over time.[37] This method is unfortunately not very useful for characterizing small Pd NPs, as they do not have a SPR peak in the visible region. Rather, they show a broad scattering profile that extends into the visible region that can be used to help confirm the presence of Pd NPs.[32] TEM and HRTEM have been used extensively as the primary methods for determining NP size, size dispersity and morphology. Additionally, HRTEM has the advantage of showing the lattice structure of NPs and any evidence of polycrystallinity. Powder x-ray diffraction can be used to confirm the crystal structure of metallic NPs. It can also be used to estimate average NP size via the Scherrer equation based on the peak broadening for crystallographic planes in the diffraction pattern.[33] For small single crystal NPs, sizes determined by XRD usually correlate well with sizes given by analysis of TEM images, although this does not apply for *polycrystalline* NPs. As will be seen in Chapter 2, XRD size determinations of polycrystalline NPs often give size estimates that are below the TEM diameter because of the smaller domain sizes of such NPs. SEM, like AFM can be used to assess the topography of NP arrays. EDS analysis can be used to assay the elemental composition of the NPs and surrounding ligands. When used in conjunction with TEM, information can be obtained about the coverage of the capping ligands on the NP surface.

General NP electrochemistry

NPs often have much different electrochemical properties than bulk materials, making them excellent candidates for electrochemical studies. A unique property of very

small, monodisperse NPs is the phenomenon of quantized double-layer (QDL) charging instead of continuous double-layer charging seen in bulk materials.[38] In QDL charging, single electron charging and discharging events are visible as distinct peaks in voltammetric experiments on NPs both in solution and attached to surfaces. In this way, NPs function as quantum capacitors. This behavior has been well studied by Murray and coworkers for silver quantum dots[39,40] as well as palladium and gold NPs.[41] Electrochemical properties are usually studied with cyclic (CV) or differential pulse voltammetry (DPV).[38] The electrochemical study of NPs is commonly facilitated by immobilizing them on an electrode surface. Immobilization methods include forming layer-by-layer (LBL) assemblies,[42-44] incorporation in Nafion membranes,[45] and electrodeposition in which the original capping ligands have been exchanged with redox-active ligands.[46]

Behavior of Bulk and Nanoscale Palladium

Palladium is well-known for to its ability to catalyze many organic coupling and hydrogenation reactions. It is also useful as a catalyst for reactions such as peroxide reduction,[47] hydrogen oxidation,[48] and alcohol oxidation in direct alcohol fuel cells.[49-51] Another useful and well-studied property of palladium metal is its ability to reversibly absorb and release hydrogen,[52] which has important uses for hydrogen purification and detection,[53] and isotope separation.[54] Although palladium can be used as a hydrogen storage material, the high cost of the metal makes this impractical. When solid Pd is in contact with hydrogen gas H_2 molecules dissociate on the Pd surface and diffuse into the Pd lattice to form PdH_x where x is the ratio of H to Pd. Hydrogen is well-known to occupy primarily octahedral sites in the face-centered cubic lattice, however there is

experimental evidence that tetrahedral sites can be occupied as well.[54] Initially PdH_x will exist solely in the α-phase up to a value of x=0.015 in which the crystal structure is preserved and there is little change in the lattice constant. Beyond that value, the PdH_x β-phase begins to form with a corresponding increase in lattice constant. The α and β phases coexist as x further increases, up to a value of x=0.6. At that point, the PdH_x exists solely in the β phase in which the hydrogen content continues to increase, up to a value of about x=0.7.[52] The maximum loading of H into Pd has important ramifications for its use in a variety of applications, and so it has been studied extensively. We show in Chapter 2 an improved electrochemical determination of x in Pd NPs.

Pd NP synthesis

There has been great interest in synthesizing palladium NPs (Pd NPs) using a variety of methods for different purposes. Murray and co-workers[23] synthesized Pd NPs capped with either hexanethiolate or dodecanethiolate using the popular Brust method with palladium tetrachloropalladate as the metal precursor. As expected, the average size decreased with an increase in the ligand:metal ratio. Interestingly, if the ligand:metal ratio was larger than 2:1, the product became a Pd(II) alkanethiolate complex instead of discrete NPs.

In a variation of the Brust synthesis, Coronado and co-workers synthesized water-soluble Pd NPs.[3] They utilized a 2-phase method in which the tetrachloropalladate ion was reduced in the organic phase to form Pd NPs with TOABr also serving as the capping ligand. The NPs dissolved in toluene were transferred to water by the addition of an aqueous solution of dimethylaminopyridine (DMAP), which is neutral in toluene but forms a zwitterion in water. This nitrogen-donor transfer agent also serves as the capping

agent for the NPs in solution. This synthesis gave NPs with sizes ranging from 0.9 to 3.5 nm.

Pd NPs have also been synthesized by thermal decomposition of molecular precursors of Pd. Hyeon and co-workers[30] prepared a Pd-trioctylphosphine (Pd-TOP) complex by reaction of Pd acetylacetonate (acac) with TOP. The Pd-TOP complex was then heated to 300 °C, causing thermal decomposition of the acac to yield CO, which was postulated to act as a reducing agent for the Pd. This method yielded very monodisperse Pd NPs with sizes of 3.5, 5, and 7 nm by varying the relative amount of TOP, with higher concentrations yielding smaller NPs. The resulting NPs were soluble in nonpolar solvents such as THF.

Evangelisti and co-workers[30] synthesized Pd NPs stabilized by PVP, which were soluble in 1-hexene/metitylene 50/50 mixtures using a technique called metal vapor synthesis. The synthesis utilized Pd metal rather than a salt as the starting material, which eliminated complications of impurities like chloride. The metal was heated to produce Pd vapor, which was then co-condensed at 77 K with a 1-hexene/mesitylene mixture followed by warming to 233 K to yield solvated Pd atoms. This solution was then added to ethanol containing PVP. An excess of diethyl ether was added to precipitate Pd NPs dispersed in PVP that were soluble in polar solvents such as alcohols and water. The sizes of NPs made in this way varied in diameter from 1-3.5 nm with a small distribution.

Many synthetic methods yield Pd NPs soluble in organic solvents such as toluene, which tend to be smaller, with very good size control. Syntheses utilizing organic methods can be environmentally disadvantageous, as many of the solvents tend to be

toxic. Recently, efforts have been focused on producing more environmentally benign water-soluble NPs, which have potential use in biological applications. Several synthetic preparations have been developed which produce monodisperse water soluble NPs with good size control.

In a variation of the organic phase MPC synthesis which utilized alkanethiolates as capping ligands, Murray and co-workers synthesized Pd MPCs in water using trimethyl(mercaptoundecyl)ammonium ligands. The synthesis was done by reducing a palladium salt (K_2PdCl_4) with sodium borohydride in the presence of the capping ligands.

Crooks and co-workers have done extensive work to synthesize aqueous Pd NPs[55,56] formed by reduction of metal ions complexed to the inside of dendrimer templates to form palladium dendrimer encapsulated NPs (Pd DENs). DENs synthesized in this way had diameters of less than two nanometers with very narrow size dispersity, with the final size of the DENs dependent on the dendrimer used. Ultraviolet-visible spectroscopic studies have shown that the as-prepared DENs are stable in a reducing environment such as hydrogen saturated aqueous solution,[55] but rapidly reoxidized in the presence of air. The DENs could be extracted from their templates with alkanethiols to form Pd MPCs, which were much more stable.[41]

Liang and co-workers[57] used photochemical reduction in aqueous solution to control the shapes of Pd NPs capped with cetyl trimethylammonium bromide (CTAB). In general, a solution of CTAB and ammonium tetrachloropalladate was stirred in water to form a complex. Ascorbic acid was added to this solution followed by irradiation with UV light (260 nm) for about 4 hours. The ascorbic acid acted as a reducing agent in the presence of UV light, producing radicals and solvated electrons due to homolytic

cleavage. Interestingly, with lower CTAB:Pd ratios, spherical particles were formed, whereas higher CTAB:Pd ratios caused the formation of Pd nanocubes and nanorods. Aqueous solutions of these nanostructures were found to be stable for several months.

Chapter 2 presents our work on the synthesis, characterization, and electrochemical hydrogen insertion in palladium NPs. A simple "one-pot" synthesis done by Brooks and co-workers utilized the nucleotide adenosine triphosphate (ATP) as a capping ligand and sodium borohydride as a reducing agent to produce water-soluble gold NPs ranging in size from 2 to 5 nm.[36] We have synthesized water-soluble Pd NPs using a similar procedure, using hydrogen tetrachloropalladate as the metal precursor. Our NPs were purified by dialysis and subsequently collected as a dry solid. They have been characterized by UV-Vis spectroscopy, TEM/HRTEM and XRD to determine their size and crystal structure, and SEM/EDX to determine their composition. A glassy carbon electrode (GCE) was loaded with Pd NPs by continuous cycling in an aqueous NP solution with potassium sulfate as the supporting electrolyte. Electrochemical experiments were performed in 1 M potassium hydroxide solution using cyclic voltammetry (CV). The hydrogen adsorption and absorption processes were studied by varying the scan rate and potential limits. Additional experiments investigated the total palladium loading on the electrode and ultimately the amount of hydrogen absorbed by the Pd NPs.

Chapter 2

SYNTHESIS, CHARACTERIZATION AND ELECTROCHEMICAL HYDROGEN INSERTION IN PALLADIUM NANOPARTICLES

Introduction:

Hydrogen is well known to be a much cleaner energy carrier than fossil fuels, and has great potential for alternative energy applications such as fuel cells. The hydrogen economy requires an effective and safe way to store and release hydrogen, as well as purify and detect it. Palladium is known to easily absorb and release hydrogen in its face-centered cubic lattice, to form PdH_x, a process that is well understood for bulk Pd.[52] Most known studies on the palladium hydrogen system have been done with gaseous hydrogen with sponge palladium. The absorption of hydrogen into the Pd lattice occurs in two distinct and well-known phases, α then β, as hydrogen content is increased. Initially, the dilute α phase is formed in which the crystal structure of the metal is preserved, and there is minimal change in molar volume. The β phase corresponds to higher hydrogen content with a distinct increase in lattice constant. At low hydrogen concentrations, PdH_x exists solely in the α phase. As the H:Pd ratio increases beyond ca. 0.015, called α_{max}, the β phase begins to form. The alpha and beta phases coexist up to $x \approx 0.6$. Beyond that point (β_{min}), the PdH_x exists completely in the β phase.[58] Studies of the PdH_x system have shown that the 2-phase behavior is temperature dependent. The range of compositions in which the α and β phases coexist in bulk Pd decreases as temperature increases, up to a critical temperature of 570K where there is no coexistence region.

Because nanoparticles can have very different size-dependent properties than their bulk counterparts due to a high specific surface area and quantized energy states, there is great interest in studying hydrogen storage properties in palladium nanoparticles (Pd NPs). Relatively recent results have shown that in nanoparticles, the alpha-beta co-existence region is much narrower than in bulk and decreases with particle size.[59] Studies have shown that hydriding and dehydriding of Pd NPs is kinetically faster than in bulk.[60,61] There is also a large reduction in critical temperature, from 570K to ca. 430K[62,63] which also decreases with NP size.[59] Some studies have suggested that the hydrogen storage capacity is increased relative to bulk samples due to a higher proportion of subsurface sites.[59,64,65] It has also been observed from molecular dynamics simulations that the heat of formation of PdH_x decreases with decreasing NP size.[65]

Besides gas-phase hydriding of Pd, there is growing interest in studying hydrogen insertion in Pd electrochemically, both in bulk and nanoscale systems. Electrochemical hydrogen insertion in Pd has been studied in nanostructured, e.g. thin film and mesoporous Pd as well as Pd NPs. There have been extensive studies of hydrogen insertion in acid, which involves fast electron transfer processes.[66-70] Czerwinski and co-workers investigated hydrogen absorption from sulfuric acid into Pd thin films deposited on gold and glassy carbon. Cyclic voltammetry experiments in acid showed a clear distinction between hydrogen adsorption and absorption in the α and β phases. They also showed that the hydrogen content in the Pd thin film depended on electrode potential.[67] Russell and co-workers also investigated the electrochemical potential dependence of hydriding palladium in Pd NPs supported on carbon using x-ray diffraction[70] and extended x-ray absorption spectroscopy[71] in sulfuric acid. The electrode potential was

held at progressively more negative voltages for a given amount of time to charge the electrode with hydrogen followed by a linear anodic sweep to reoxidize the hydrogen absorbed in the Pd. Their results have shown that hydrogen content was dependent on electrode potential, and they were able to distinguish between the alpha, beta, and coexistence regions voltammetrically. Similar work was performed by Bartlett and co-workers in acid using nanostructured Pd films electrodeposited on gold.[68,72] Lasia and co-workers also investigated hydrogen insertion in Pd films of varying thickness using cyclic voltammetry. They found that there was a strong dependence of the film thickness on the hydriding kinetics as well as the separation of voltammetric peaks corresponding to hydrogen adsorption, absorption in the Pd lattice and hydrogen evolution.[69,73] Similar experiments comparing vacuum-deposited Pd NPs to a Pd wire have shown that the hydrogen peaks could be resolved with NPs but not with bulk Pd.[74] Relatively few studies have been conducted to investigate hydrogen insertion in base, with most studies focusing on Pd thin films[75,76] and mesoporous Pd[77] with even fewer studies on Pd NPs.[74] Electrochemical hydrogen insertion was studied in base by Pletcher and co-workers[77] for nanostructured Pd deposited on platinum. They showed better-resolved peaks for the hydrogen insertion, desorption and evolution processes in the films compared to bulk Pd, however the processes involved a slower electron transfer than experiments done in acid.

There has been great interest in synthesizing monodisperse Pd NPs with controllable size so that their size-dependent properties can be studied for hydrogen storage as well as catalytic applications. Some syntheses of Pd NPs involve a phase transfer from water to organic media.[3] Pd NPs have been stabilized using polymers such as polyvinylpyrrolidone[28,30,31,78,79] which can difficult to remove making electrochemical

experiments impractical. They have also been synthesized by encapsulation in dendrimer templates.[55,56,80] Vacuum deposition has been utilized to produce Pd NPs directly onto a glassy carbon electrode without the need for capping ligands.[81]

We describe a more environmentally friendly approach to synthesize water-soluble Pd NPs, which are stable against aggregation, but can also be stored as a solid. Adenosine triphosphate is used as a capping ligand, following a synthesis for gold NPs, which yielded small gold particles with good size dispersity.[36] ATP has also been used to synthesize cadmium sulfide NPs.[82] ATP-capped NPs are stable because of the large electrostatic repulsion due to negatively charged phosphate groups. ATP has the added benefit of being easily removed in order to activate the NP surface for electrochemical experiments. The presence of surface adsorbates suppresses hydrogen adsorption on the Pd surface,[72,73] so a stabilizing ligand that can be readily removed is desired. Electrochemical hydrogen insertion in the Pd NPs is investigated in basic solution using cyclic voltammetry.

Experimental Details:

Synthesis and Purification of Nanoparticles

The Pd NP synthesis was adapted from a preparation used to synthesize stable nucleotide-capped gold nanoparticles.[36] In a typical synthesis, palladium (II) was reduced by sodium borohydride in the presence of ATP. Adenosine-5'-triphosphate disodium salt (99%,) and sodium borohydride (99.9%) were purchased from Aldrich. Anhydrous palladium (II) chloride (99.9%) was purchased from Strem. Millipore water of resistance 18.3 MΩ was used for all syntheses. Palladium chloride was dissolved in a stoichiometric amount of hydrochloric acid to form the tetrachloropalladate ion. In a typical synthesis,

H_2PdCl_4 (25 mL, 10 mM) and ATP (10 mL, 25 mM) were added to 955 mL of Millipore water to give a final Pd^{2+} concentration of 250 μM with a Pd:ATP:$NaBH_4$ ratio of 1:1:10. The Pd:ATP:$NaBH_4$ ratio was varied in order to try to control the average particle size.

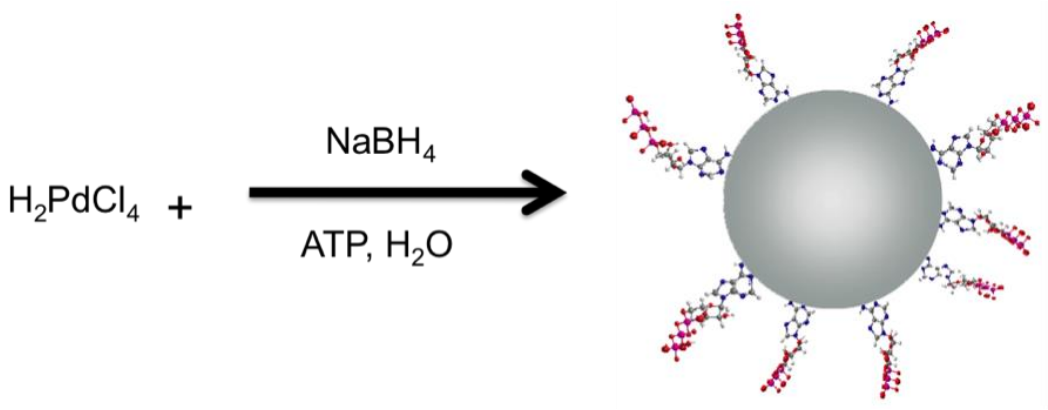

Figure 1. Schematic representation of the formation of ATP-Capped water soluble palladium nanoparticles

The concentration of Pd(II) in the synthetic solution was held at 0.250 mM for the majority of experiments . From this point forward, the particle solutions will be identified by the Pd:ATP:$NaBH_4$ ratio used for the solutions in which the initial Pd^{2+} concentration is 250 μM. For all others, the Pd^{2+} concentration will be specified. The Pd^{2+} + ATP solution was stirred at room temperature for ~30 minutes. A freshly prepared solution of $NaBH_4$ (10 mL, 100 mM) was added to reduce the Pd (II) to Pd (0). An immediate color change from pale yellow to light brown indicated nucleation of NPs. Over 3 hours this solution gradually changed to a darker brown, indicating particle growth. The particle solution was stirred under an N_2 atmosphere for 6 hours after reduction to allow for particle growth. The solution volume was then reduced to ~15 mL by rotary evaporation, and the NP solution was purified by dialysis. Cellulose dialysis tubing purchased from Spectrapor with molecular weight cutoff of 10,000 was used.

Dialysis was performed in 3.0 L of deionized water, with the water being changed every 24 hours for a total of 96 hours. The presence of free ATP in the dialysis water was monitored by UV-Vis spectroscopy. The particle solution was then further concentrated by rotary evaporation to 3 mL. Isopropyl alcohol (IPA, 0.1 mL) was added to precipitate the solid particles. The supernatant solution was removed, and the solid powder was dried under N_2.

Size-selective precipitation:

The 1:5:10 batch was chosen to attempt a size-selective precipitation using a method adapted for monodisperse CdS nanoparticles.[83] The method utilizes solubility differences for nanoparticles of varying sizes. A 50 μl aliquot of IPA was added to the concentrated particle solution after it had been removed from dialysis, precipitating a small fraction of the nanoparticles. The solution was centrifuged and the supernatant solution (labeled supernatant 1) was separated from the solid particle powder (labeled initial precipitation), which was subsequently dried under N_2. The solution was re-concentrated and a small aliquot of IPA was added to the solution to precipitate the remaining particles.

Characterization:

The particles were characterized by transmission electron microscopy (TEM) and high-resolution TEM to determine average particle size and distribution. X-ray powder diffraction was used to confirm the crystal structure of the Pd NPs as well as correlate the particle size to the TEM. Scanning electron microscopy with energy dispersive x-ray analysis spectroscopy was used to determine the number of capping ligands per particle,

as well as estimate the projected molecular area of each ligand on the particle surface. Ultraviolet-visible spectroscopy was used confirm the presence of Pd NPs in solution.

TEM:

Sample preparation was done by dissolving 0.1 mg of the cleaned Pd NP powder in 10 mL of 18.2 MΩ water, which was then sonicated for 5 minutes. 6.0 μL of this solution was dropped on a 400-mesh Formvar coated copper TEM grid and allowed to dry for 10 minutes. The excess solution was removed from the grid with a piece of filter paper, and the grid was dried under nitrogen. TEM imaging was done with a Philips CM-12 electron microscope operated in bright field at 80 keV. High-resolution electron microscopy was done on a JEOL 2010f microscope operated at 200 keV. The TEM data were analyzed by measuring the diameters of at least 75 randomly selected particles per batch using ImageJ software.

X-ray diffraction:

X-ray diffraction studies were performed on a Siemens D5000 powder diffractometer with an x-ray wavelength of 1.54056 Å (CuKα1). Samples were prepared by dispersing ca. 5 mg of a cleaned Pd NP powder in ethanol and transferring the powder onto a zero-background quartz sample holder. The ethanol was then allowed to dry in air. Experiments were run for 34 minutes in the angle range $5 \leq 2\theta \leq 90$ degrees.

SEM/EDS:

Scanning electron microscopy was performed on a XL30 ESEM-FEG with attached energy dispersive x-ray analysis (EDS). Sample preparation was done by attaching a small grain of nanoparticle powder to double-sided carbon tape. The EDS spectrum was used to determine the elemental composition of the ATP-capped Pd NPs,

similar to methods used for bimetallic NPs.[84] The EDS spectrum gave the atomic ratio of palladium to phosphorus, which was used to estimate the number of ATP molecules per nanoparticle.

UV-Vis: 2 mL of the synthetic prep were diluted to 5 mL (0.1 mM Pd^{2+}). Spectra were collected before and after reduction from 200 to 800 nm using an Ocean Optics spectrometer (HR4000CG-UV-NIR). Samples were contained in a 1 cm open quartz cuvette.

Electrochemistry:

The 1:1:10 NP batch was the most thoroughly characterized, and therefore was selected for electrochemical experiments. All experiments were performed using a CHI 760c potentiostat. A 3 mm diameter glassy carbon electrode (GCE) purchased from CH Instruments was used as the working electrode in all experiments. A coiled platinum wire and Ag/AgCl electrode (+0.235 V vs. SHE) were used as the counter and reference electrodes respectively. Prior to electrochemical experiments, the GCE was polished with a 0.05 μm α-alumina water slurry, sonicated for 5 minutes and rinsed thoroughly with 18.3 MΩ water. Pd NPs were attached to the GCE by continuous cycling in a 25 μg/mL particle solution in 0.1 M K_2SO_4. The prepared GCE was rinsed thoroughly and used for further CV experiments in 1 M KOH.

Table 1 shows the various Pd:ATP:$NaBH_4$ ratios used in the synthesis of the NPs as well as sizes determined by TEM analysis. In general, a higher ATP:Pd ratio favors the production of smaller and more monodisperse particles which is consistent with findings for ATP-capped gold particles.[36] A higher ratio of stabilizing ligand is better able to prevent further particle growth. In addition, samples with a higher $NaBH_4$:Pd ratio had

smaller particles, possibly due to more rapid reduction of Pd(II) resulting in the formation of more nuclei. The fractional precipitation for the (1:5:10) NPs suggests that larger particles will precipitate first, leaving smaller particles in the supernatant solution.

Pd:ATP:$NaBH_4$ Ratio	H_2PdCl_4 (10 mM) /mL	ATP (10 mM) /mL	$NaBH_4$ (mg) in 10mL H_2O	$[Pd^{2+}]$ /mM	NP Diameter /nm
1:1:20	25.00	25.00	94.6	0.250	3.0±0.4
1:1:5 Initial precipitation	25.00	25.00	23.6	0.250	2.3±0.4
1:5:20	25.00	125.00	94.6	0.250	2.5±0.3
1:1:10	25.00	25.00	47.3	0.250	3.6±0.6
1:0.5:10	25.00	12.50	47.3	0.250	3.4±0.5
1:0.5:15	25.00	12.50	71.0	0.250	3.1±0.5
1:5:10 initial precipitation	25.00	125.00	47.3	0.250	3.2±0.4
1:5:10 supernatant 1	25.00	125.00	47.3	0.250	2.8±0.4
1:0.5:10 125μM	12.50	6.25	23.6	0.125	3.7±0.7
1:0.5:15 125μM	12.50	6.25	35.5	0.125	3.0±0.6
1:1:10 125μM	12.50	12.50	23.6	0.125	3.4±0.7

Table 1. Synthesis of Pd NPs by varying Pd:ATP:$NaBH_4$ ratios with sizes determined by TEM, Total Volume=1000 mL

Results and Discussion:

Ultraviolet-visible spectroscopy

Figure 2 shows the UV-Visible spectrum of the diluted 1:1:10 NP solution before and after reduction. The large peak at ca. 260 nm is from ATP.[85] Before reduction, a slight shoulder is visible at ca. 300 nm, which comes from the $PdCl_4^{2-}$ complex.[3] After reduction, there is a broad increase in the absorbance of the solution with a tail extending into the visible region, which is responsible for the brown color of the NP solution. Unlike other metallic NPs such as gold and silver, which exhibit a characteristic surface

plasmon resonance peak (SPR) in the visible region that can be utilized to some degree to estimate particle size and morphology, palladium has a SPR band in the UV close to 200 nm which could not be observed due to experimental limitations. Instead, there is a Mie scattering profile extending into the visible region consistent with the calculated spectrum for Pd NPs.[32] The spectrum is also consistent with experimental results for small (< 3 nm) thiol-capped[23], dendrimer encapsulated[55,80] Pd NPs and DMAP-capped Pd NPs.[3]

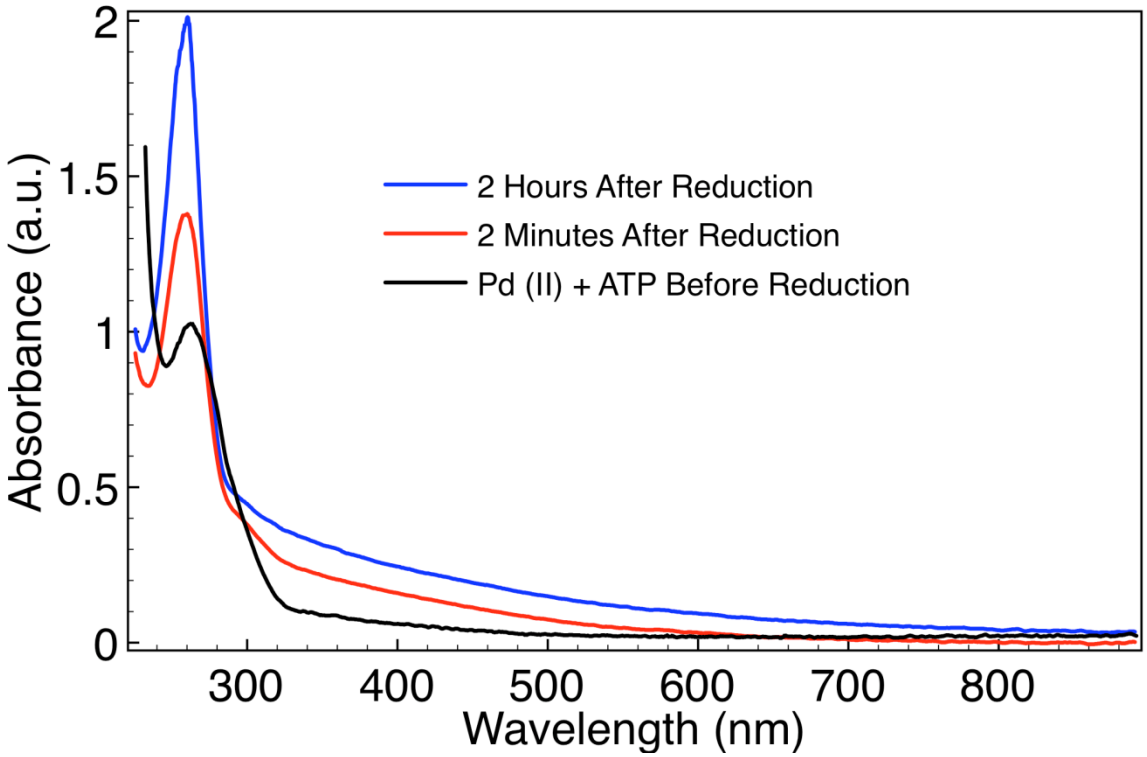

Figure 2. UV-Vis spectrum of 1:1:10 Pd NP solution before and after reduction

TEM and HRTEM

Figure 3 shows a representative TEM image of NPs produced from the 1:1:10 Pd:ATP:BH_4^- synthesis. The particles are fairly small with a narrow size distribution. For N=100, the average diameter is 3.6±0.6 nm. Some aggregation occurs during synthesis, as can be seen in the TEM and HRTEM images. In the TEM image (Figure 3) some fusing and elongation of the Pd NPs can be seen. The high-resolution TEM image

(Figure 4) shows a larger aggregate with lattice fringes oriented in several directions. This aggregative growth behavior has been observed for silver nanoparticles.[86,19,87] There is some contamination from excess ATP that could not be removed by purification, as is shown by the web-like features surrounding the Pd NPs.

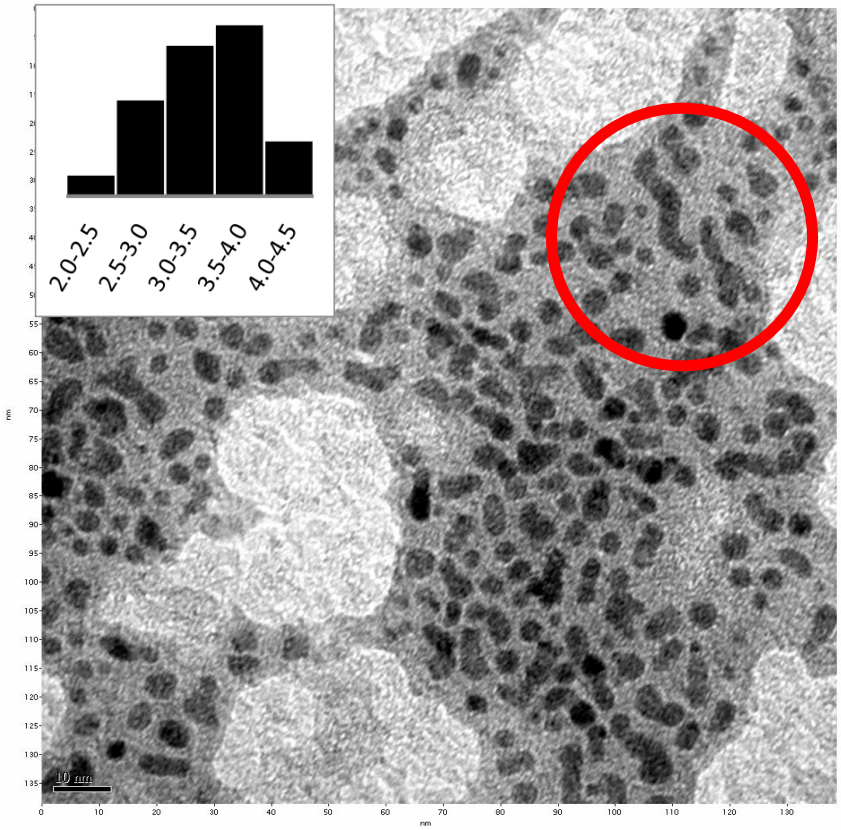

Figure 3. Representative TEM image and (inset) histogram of cleaned Pd NP. Pd:ATP:$NaBH_4$ ratio = 1:1:10, scale bar = 10 nm.

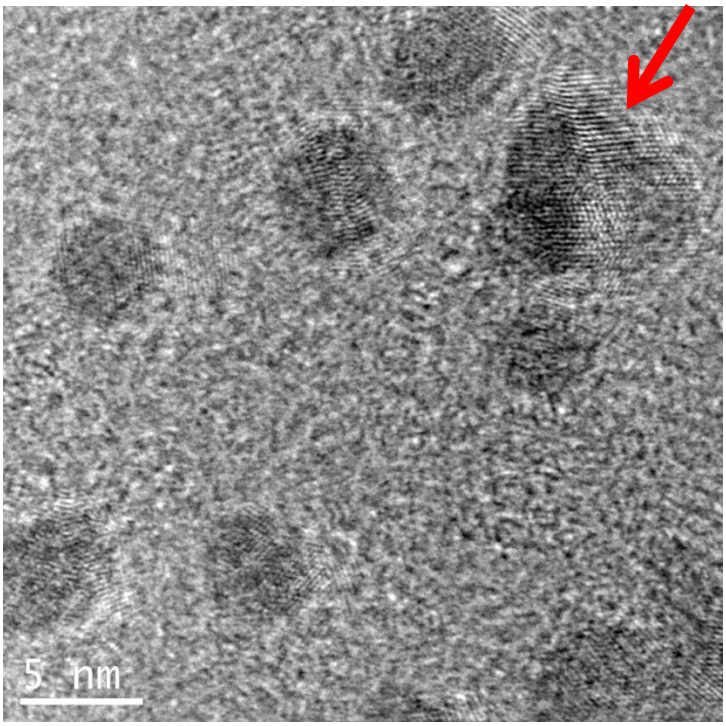

Figure 4. HRTEM of 1:1:10 Pd NPs showing polycrystalline structure of Pd NPs, scale bar = 5 nm

X-ray diffraction

The x-ray diffraction pattern (Figure 5) confirms the face-centered cubic (fcc) structure of palladium.[88] The nanoparticle grain size was estimated by the Scherrer equation[33] using the full-width at half-maximum (FWHM) of the Pd [2 2 0] peak and shape factor, K, of 0.9. The average size was 0.971 nm, much smaller than the size determined by TEM measurements, which further suggests some growth via an aggregative mechanism. Analysis of other samples shows a similar trend, with the size given by XRD being much smaller than the size determined by XRD analysis. The peaks in the Pd NP diffraction pattern are shifted to lower angles with respect to the bulk (shown as red lines in the Figure). The Pd NP lattice constant calculated from the position of the [1 1 1] peak was 3.93 Å, while that for bulk Pd is 3.89 Å. This is the opposite behavior of what is expected for metallic NPs, where the lattice parameter

usually decreases vs bulk due to surface tension effects.[89] Lattice contraction with decreasing particle size has been reported for pure Pd NPs,[90,91] however several reports have shown a lattice expansion for Pd NPs vs. bulk due to the presence of impurities such as hydrogen, oxygen or carbon, or pseudomorphism due to substrate effects.[90,92] In the case of the ATP capped Pd NPs it is likely that the presence of the ATP would relieve some of the stress due to uncoordinated Pd atoms at the NP surface, lessening the lattice contraction. Another explanation supposes that NP systems exposed to air will develop a partial oxide layer on the surface and possibly in subsurface sites.[93] The presence of a residual surface oxide could cause a lattice expansion in the Pd NPs, which has been suggested by Ingham and coworkers.[92] Other investigations studying gaseous hydrogen uptake in Pd NPs using XRD have noticed a similar phenomenon and observed that surface oxide would block hydrogen adsorption sites.[62] A previous study by Coronado and coworkers reported XPS evidence for palladium oxide at the surfaces of DMAP-capped NPs, consistent with the notion that surface oxidation is relatively common.[3]

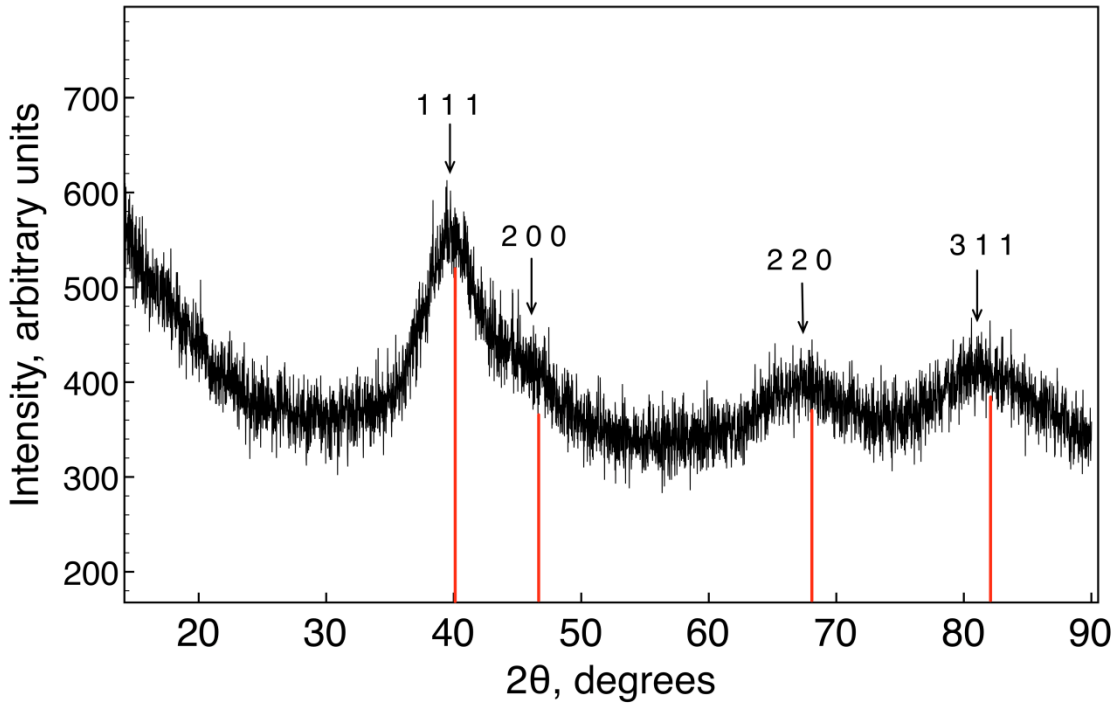

Figure 5: Powder X-Ray diffraction pattern showing the face-centered cubic structure of Pd, with red lines indicating peak positions in bulk Pd

STEM

The NPs were also characterized by scanning transmission electron microscopy (STEM, Figure 6) which has been used to characterize Au (core) Pd (shell) NPs[94] as well as on oxide supported Pd NPs.[95] The advantage of this method is that it gives contrast of elements based on their z-number, allowing for a better determination of the NP shape. In the case of Pd NPs (z = 46) Pd is clearly seen while ATP is absent from both the STEM and HRTEM due to destruction by the high-energy electron beam. Sizes from the STEM image are in good agreement with sizes from TEM. It is also evident that there is some agglomeration and/or elongation of the NPs, which may hint at the formation of some Pd nanorods, although it is not clear if growth is favored along a particular crystallographic axis. Shape-controlled synthesis of Pd nanostructures (PdNS) has been explored in several studies.[57] Xia and co-workers were able to synthesize various shapes

of metal NSs in water by: 1) controlling the crystallinity of NS seeds (single crystal vs. twinned) by varying the reduction rate of the NS precursors and 2) the growth rate of specific crystallographic facets by selecting capping ligands which preferentially stabilize certain facets over the others. In the case of nanorods, single-crystal seeds were generated by fast reduction of the Pd precursor and preferential stabilization of the [1 0 0] facets, allowing growth along the [1 1 1] facet.[14,96] Both of these reports describe a mixture of different NS shapes, with one being dominant. A more complete understanding of the binding energy of ATP to specific crystallographic facets of Pd is needed to assert if nanorods are indeed being formed.

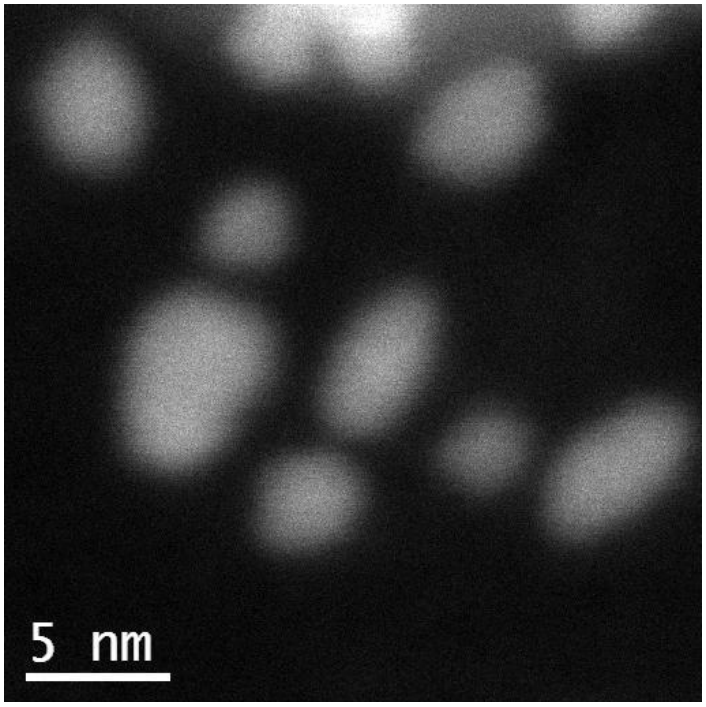

Figure 6: Scanning TEM image of 1:1:10 with Z-contrast

SEM/EDS

The cleaned and dried NP powders were also characterized with SEM/EDS for elemental analysis. The EDS spectrum is shown in Figure 7, while Table 2 shows the

atomic and mass percentages for the elements in the sample. The small peak at ca. 1 keV corresponds to sodium counterions for the phosphate groups on the ATP. The low-energy carbon signal comes from the carbon tape holding the sample. The large sample size means that the atomic ratios given by this method can be assumed to represent the approximate overall elemental composition of the powder. The phosphorous to palladium ratio and the average particle sizes were used to estimate both the number of ATP molecules per particle and the projected molecular area per ATP on the particle surface. For instance, a spherical Pd NP with TEM diameter of 3.6 nm has a volume of $2.44X10^{-20}$ cm^3 and surface area of 40.7 nm^2. Since the density of Pd is 12.02 g/cm^3, the particle has a mass of $2.44X10^{-19}$ g and contains 1662 Pd atoms. If the P:Pd ratio is 0.2, the NP is capped by ~117 ATP molecules, assuming that the ATP does not undergo significant hydrolysis to form adenosine diphosphate (ADP) or adenosine monophosphate (AMP), which would lower the measured P:Pd ratio and cause the calculated ATP surface area to be too high. This corresponds to a molecular area per ATP molecule of 0.34 nm^2, which is comparable to an area of 0.44 nm^2 per adsorbed adenine on gold surfaces determined by Prado and coworkers using surface excess values.[97,98] The binding interaction between gold and adenosine monophosphate (AMP) were studied by Kundu and coworkers using surface enhanced Raman spectroscopy (SERS) and surface enhanced infrared absorption spectroscopy (SEIRA). Their results suggest AMP binding to gold through the N7 ring nitrogen with the exocyclic NH_2 group lying close to the gold surface.[98] Giese and coworkers also used SERS along with density functional theory (DFT) calculations to confirm that adenine adsorbs to silver surfaces in the same way.[99] Studies on the binding energy and orientation of adenosine on

palladium surfaces have not been reported, but it is reasonable to assume that there is a similar interaction between the ATP and palladium since both ATP and adenine have the same binding group. This particular orientation of the ATP molecule, with the negatively charged phosphate groups oriented away from the NP surface would protect the NPs against aggregation due to strong electrostatic repulsion, which is consistent with the behavior of the particles in aqueous solution. The NPs can also be dissolved in water after being isolated as a solid. If free ATP exists in the NP powder, the measured P:Pd ratio would be too high and the calculated surface area occupied by each ATP molecule will be too low. TEM data shows there is indeed ATP left over after dialysis, so the calculated surface area of 0.34 nm^2 is lower than expected for an end-on orientation. The presence of contamination in the form of excess ligand makes it difficult to determine the surface area occupied by each ligand and by extension their orientation, however, as mentioned previously, it is reasonable to assume a similar orientation for ATP on Pd as for Au and Ag.

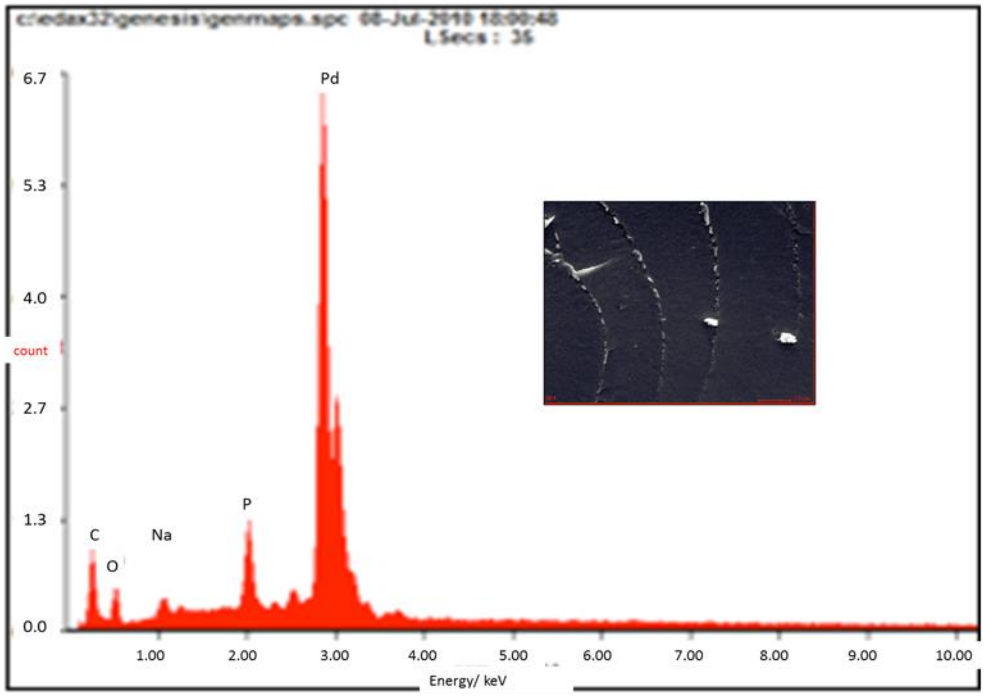

Figure 7: EDS spectrum of cleaned 1:1:10 NP powder showing elemental composition. Inset shows the area of PdNP powder used for analysis.

Element	Wt%	At%
CK	15.2	46.4
OK	09.5	21.6
NaK	02.1	03.3
PK	04.2	05.0
PdL	69.0	23.7

Table 2: Elemental composition of 1:1:10 purified Pd NPs from EDS analysis

NP Deposition on GCE

Unless otherwise specified, all currents and charges are given with respect to the GCE surface area. In order to investigate the electrochemical hydrogen insertion properties of the Pd NPs, the NPs were first attached to a glassy carbon working electrode using a novel electrodeposition technique. The working electrode was continuously cycled in a dilute NP solution from -1.2V to 0.6V vs. Ag/AgCl, at 100 mV/s with 0.1 M K_2SO_4 supporting electrolyte. Figure 8 shows particle deposition on a GCE by continuous cycling over 24 complete cycles. It was found that after several cycles

particles began attaching to the electrode surface, which was evident by the presence of voltammetric signatures at ca. 0.27 V (A1) and -0.11 V (C1) corresponding to palladium oxide formation and the subsequent oxide stripping, respectively.[74, 100,101] These peaks grow with the number of successive cycles, indicating an increase in Pd loading on the electrode over time. It has been observed that electrochemical oxide formation in silver NPs causes the loss of the ATP ligands from the NP surfaces, so it can be assumed that the NP oxidation during deposition results in NPs free of adsorbed ATP.[102] In order to study hydrogen insertion into the Pd NPs, the NP surface should be free of surface species, which may block hydrogen adsorption, as was seen from studies in which the Pd surface was poisoned with crystal violet.[72,73] The presence of the hydrogen adsorption peak (C2) suggests the NP surfaces are free of adsorbed ATP. The cathodic peaks at -0.68 V (C2) and beginning at -0.81 V (C3) have been assigned to adsorption of hydrogen onto the palladium surface followed by absorption into the palladium lattice, respectively.[74,77] As the potential is made more negative, there is a large current rise (C4) corresponding to the evolution of molecular hydrogen from the NP surface. In the anodic scan, a large peak is visible at ca. -0.45 V (A3) with a small shoulder (A4) on the negative side. The shoulder corresponds to the oxidation of molecular hydrogen while peak A3 corresponds to desorption of hydrogen from the Pd bulk, similar to experiments done using Pd NPs electrodeposited on a GCE in base.[74] Peak A2 at ca. -0.2 V corresponds to desorption of hydrogen from the Pd surface, as has been observed in several studies.[76,77] Electrochemical hydrogen insertion occurs during deposition in sulfate solution, however the peaks are not clearly resolved. The next section describes electrochemical hydrogen insertion experiments in basic solution. As will be seen, the

peaks for hydrogen adsorption and absorption are more clearly defined. Additionally, significant molecular hydrogen evolution is largely avoided, allowing for better resolution of peaks A3 and A2 corresponding to hydrogen desorption from the NP interior and surface respectively.

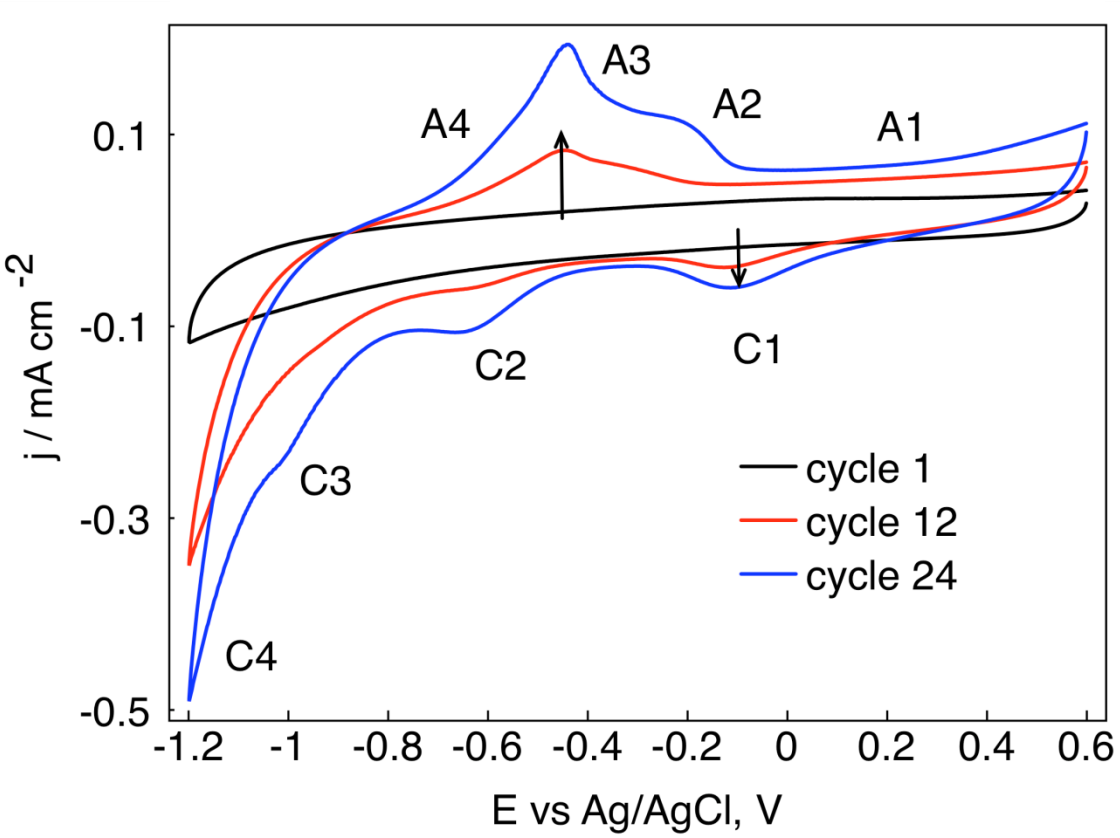

Figure 8. Deposition of Pd NPs (25 μg/ml) in 0.1 M K_2SO_4 solution in the potential range -1.2 V to 0.6 V vs. Ag/AgCl. Scan rate=100 mV/s

Hydrogen absorption in carbon-supported palladium has been well studied with both gaseous hydrogen and electrochemically.[60,70,71,74,103-105] The electrochemical hydrogen insertion behavior of the Pd NPs was studied in basic solution. The Pd NP-modified electrode was thoroughly rinsed and transferred to a 1 M KOH solution. Cyclic voltammetric experiments were performed in the range -1.4 V to 0.35 V in the hydrogen adsorption/desorption region with varied scan rate to determine which cathodic peaks

correspond to which anodic peaks. Experiments in which the scan rate was held constant and the cathodic potential limit was varied were used to investigate the dependence of the hydrogen content in the NPs on the potential.

Representative CV of NPs in base

Figure 9 shows a typical cyclic voltammogram for the Pd NP-modified glassy carbon electrode in 1 M KOH. It shares many features in common with published results for electrochemistry of palladium in base,[74-77,100,106,107] proving that the NPs can be firmly attached to the GCE using the above method. The broad anodic peak A1 from ca. -0.37 V to ca. 0.32 V and the corresponding cathodic peak C_1 at -0.38 V, which were seen during the NP deposition are well known to be the formation of palladium oxide and the subsequent oxide stripping.[100,101,107] As the potential is scanned further negative, another cathodic peak (C2) is visible at -0.9 V which corresponds to the reduction of water to form hydroxide and an adsorbed hydrogen atom:[74,108]

$$H_2O + 1e^- \rightarrow H_{ad} + OH^- \qquad (1)$$

At more negative potentials, there is a current rise beginning at -0.6 V (C3) which has been identified as the absorption of hydrogen into the Pd lattice.[68-70] The scan was reversed before the insertion process was complete and before molecular hydrogen evolution. In-situ EXAFS studies in acid identified peak C3 as the formation of β-phase PdH_x.[70] With further negative scanning, hydrogen evolution occurs, with its re-oxidation being seen as a shoulder on the A3 peak when the negative limit is extended to -1.4 V. On the return scan, peak A3 appears at -0.66 V corresponding to the re-oxidation of the β-phase PdH_x. Two peaks, labeled A2 and A2' are visible near 0.5 V, which have been observed for nanostructured Pd in base.[74,75,77,108] These two anodic peaks are believed to

originate from two different types of adsorbed hydrogen[74] Pletcher and co-workers have suggested that hydrogen is first adsorbed in C2 followed by rapid interconversion between hydrogen atoms adsorbed on the surface and subsurface hydrogen atoms.[77] An alternative explanation is that a place-exchange occurs between surface hydrogen and Pd atoms, similar to oxide layer formation in precious metals, which results in rearrangement of the surface layer.[109] In either case, the adsorbed hydrogen is oxidized at two slightly different potentials.[77] Integration of C_2 and $A_2 + A_2$' at 100 mV/s gives charges of 87.3 μCcm^{-2} and 77.5 μCcm^{-2}, respectively, for a charge efficiency ratio of 0.89, strongly suggesting that A2 and A2' correspond to oxidation of adsorbed hydrogen. The surface adsorption and desorption peaks will be investigated further in the next section.

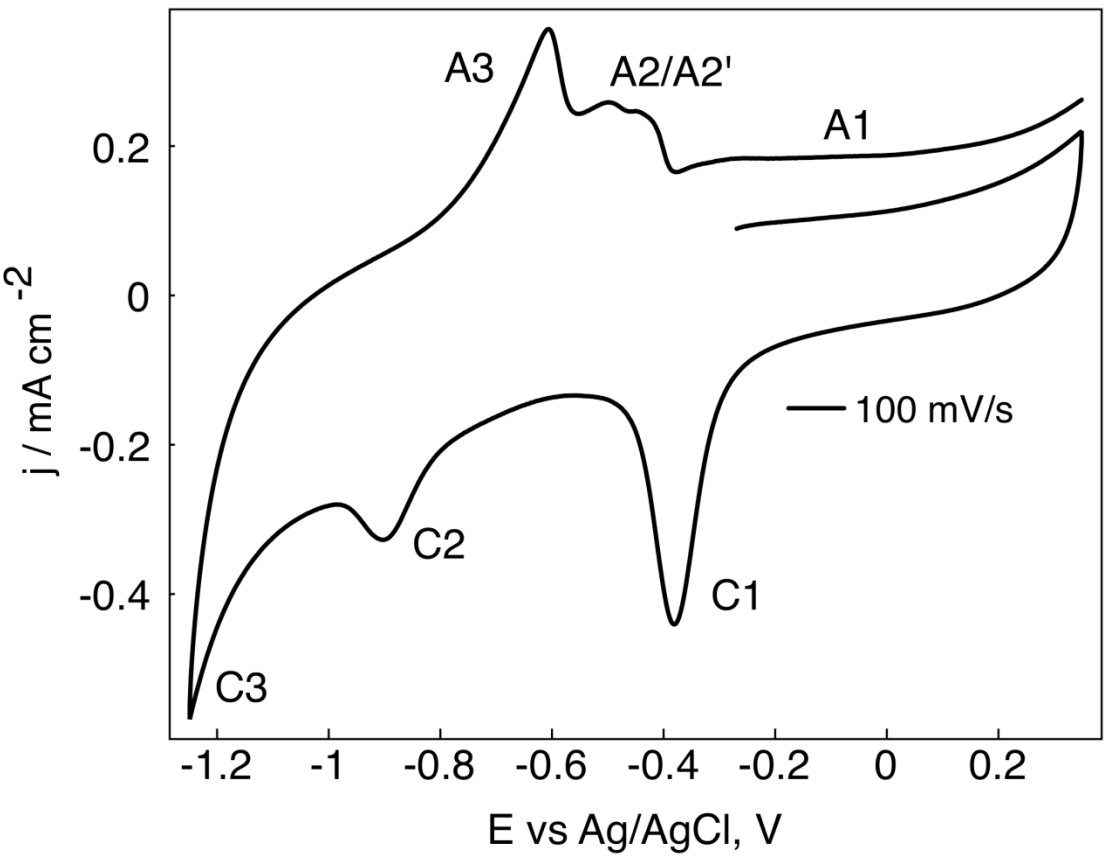

Figure 9. Representative CV of a PdNP modified glassy carbon electrode in 1 M KOH from -1.2 V to 0.35 V vs. Ag/AgCl. Scan rate=100 mV/s

Effect of scan rate in hydrogen adsorption region

The effect of scan rate was investigated in the region of hydrogen adsorption and desorption (Figure 10). The scan rate was varied from 100 mV/s to 500 mV/s. To avoid interference from anodic peaks corresponding to hydrogen desorption from the NP bulk, the scan was reversed before absorption could occur. As in Figure 9, peak C2 corresponds to hydrogen adsorption on the NP surface while A2 and A2' correspond to desorption of hydrogen from the surface. As the scan rate is increased from 100 mV/s to 500 mV/s, the potential at which C2 occurs shifts from -0.81 V to -0.91 V. A2 and A2' shift to more positive potentials, with A2' shifting from -0.45 V to -0.38 V. The increasing potential separation of the peaks indicates a slow electron transfer process for

adsorption/desorption. Additionally, A2' grows more rapidly at higher scan rates, which has been attributed by Pletcher and co-workers to interconversion between two types of adsorbed hydrogen.[77] Takasu has observed similar behavior, with the split desorption peak shifting to more positive potentials, while the more positive peak grew at the expense of the less positive peak.[81]

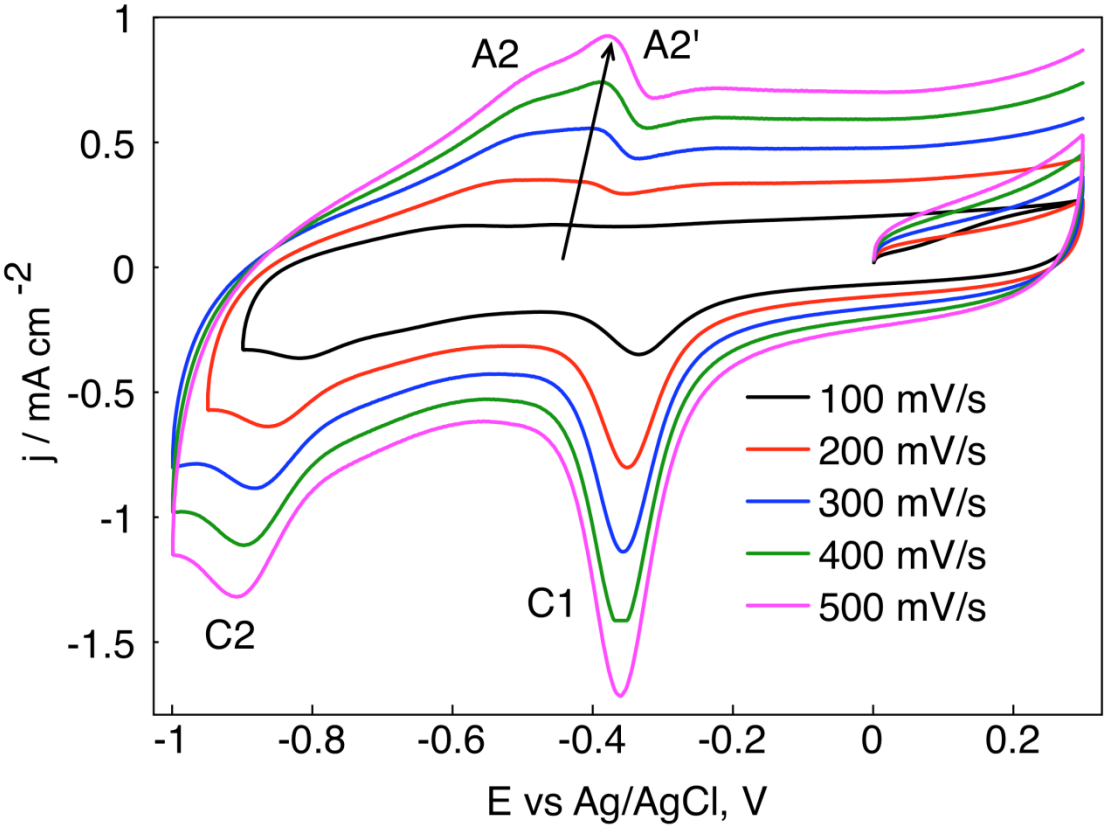

Figure. 10. CV of PdNP modified GCE in 1 M KOH with the scan rate varied between 100 mV/s and 500 mV/s. The anodic scan limit was held at 0.35 V while the cathodic scan limit was adjusted to allow for complete adsorption and minimal uptake of H into the Pd Lattice

Effect of scan rate on hydrogen insertion

Figure 11 shows experiments in which the scan rate was varied with the potential limits held constant, with the negative scan limit in the region of hydrogen insertion (-1.3

V). The palladium oxide stripping peak current scales linearly with scan rate while the peak potential is constant, indicative of a surface process. Peak C2 shifts to more negative potentials and broadens, while A2 and A2' shift toward positive potentials and broaden, which is characteristic of a slow electron transfer process. The same is true for C3/A3, since they correspond to hydrogen absorption and de-insertion, respectively. With a sufficiently high scan rate, A3 becomes so large and positively shifted that it overlaps with and obscures the desorption peaks. The positive shift in peak A3 with increasing scan rate has been observed by Takasu and co-workers.[81] The absorption and desorption peaks from the NP bulk encompass both the alpha and beta phases and the α-β phase transition. In both the alpha and beta single phases, hydrogen diffusion is very fast, with diffusion coefficients of $2X10^{-7}$ and $2X10^{-6}$ cm^2s^{-1} respectively.[110,111] The time required for hydrogen entry or exit in the β phase is therefore ~0.45μs for a 3 nm particle, so the peak shift cannot arise from hydrogen diffusion in either phase. Impedance spectroscopy measurements[112] and time-resolved studies employing EXAFS[71] have shown that the α-β phase transition is kinetically slower, which would be responsible for the increasing peak separation at increasing scan rates.

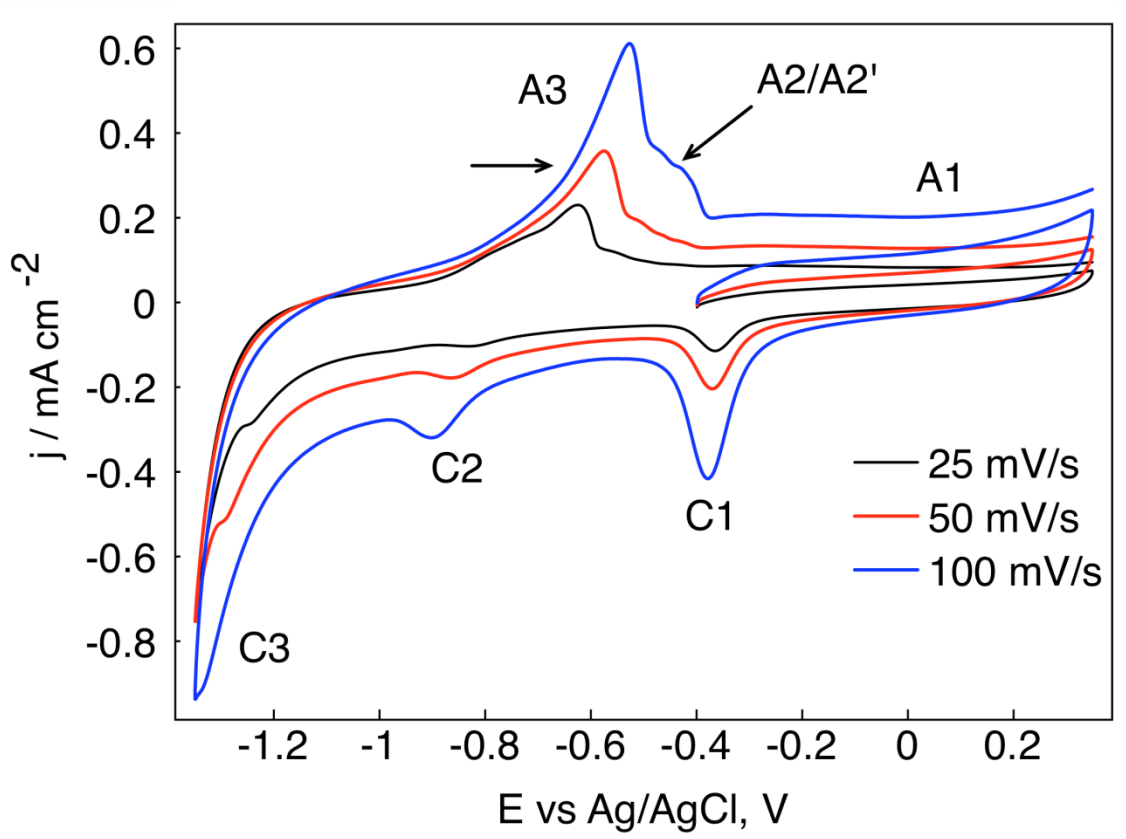

Figure. 11. CV of PdNP modified GCE in 1 M KOH with scan rate varied between 25 mV/s and 100 mV/s. Scan limits: -1.3 V and 0.35 V.

Varying the cathodic scanning limit

In order to determine which cathodic peaks correspond to which anodic peaks, the negative scan limit was varied while holding the positive scan limit at 0.35 V with a scan rate of 100 mV/s. As the potential is made more negative (Figure 12), an increase in magnitude and broadening of A3 are observed which are due to an increase in the amount of hydrogen in the Pd lattice.[70] The peak also shifts to more positive potentials, indicating a slow process. This is likely due to the movement of the alpha/beta phase boundary through the palladium lattice which involves a change in lattice parameter, and has been observed for nanostructured Pd in base[77] and acid.[69] As can also be seen from the figure, the peak intensity of C1 gradually decreases after several scans, indicating a small loss of

Pd. This can be a result of either the NPs detaching from the GCE surface, or the slow dissolution of Pd over time. It has been found that cycling through the oxide and stripping processes causes some dissolution of Pd from the NP surface although not as quickly as in acidic media.[100,101,107,108] The charge of the anodic peak corresponding to a certain cathodic scan limit can be used in conjunction with the total amount of Pd to determine the dependence of the H:Pd ratio on potential.

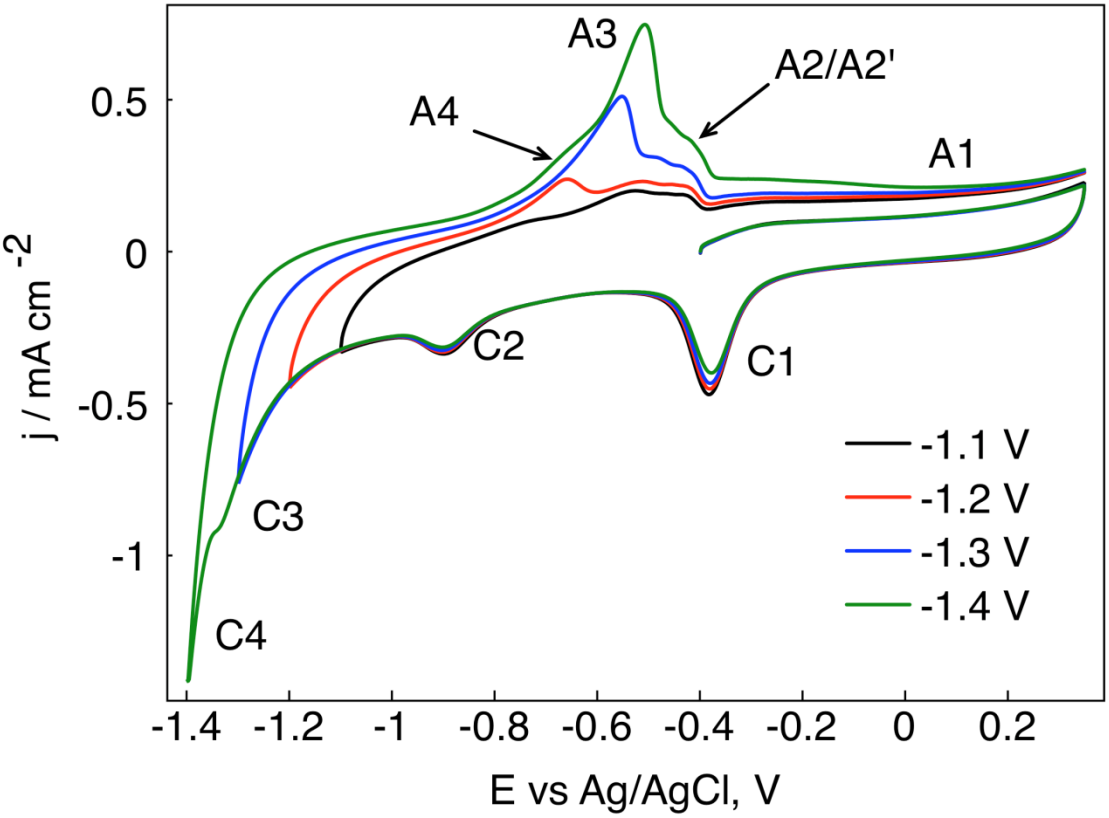

Figure. 12. CV of PdNP modified GCE in 1 M KOH with varied cathodic limit. Anodic limit = 0.35 V. Scan rate =100 mV/s

Determining Pd surface area

If the total surface area of Pd on the electrode is known, it can be used in conjunction with the NP size to determine the total amount of Pd and the number of NPs

per unit area on the GCE. Underpotential deposition (UPD) of copper on palladium can be used to assay the active surface area of Pd electrodes.[113,114] While this method is useful for determining the surface area of single crystal Pd surfaces, UPD on polycrystalline Pd is complicated, and involves bulk deposition of Cu before a monolayer is complete. Alternatively, the surface area of Pd can be determined from the reduction charge for of the surface oxide.[115,116] This was done by increasing the anodic scanning limit stepwise from 0.1 V to 0.85 V followed by complete oxide reduction. Figure 13a shows the effect of the anodic potential limit on the oxide reduction peak, which shifts towards negative potentials and increases in intensity as the anodic scanning limit is made more positive. Plotting the oxide reduction charge against the anodic potential limit (Figure. 13b) yields a straight line for potentials less than ca. 0.69 V. At more positive potentials, the slope of the line increases. It is generally accepted that the point at which the slope changes corresponds to the formation of an oxide monolayer on palladium surfaces.[115,117] The oxide reduction charge at the inflection potential of 0.69 V is 0.62mC cm^{-2} of the electrode surface area. Since the surface area of the GCE is 0.071 cm^2, the total PdO reduction charge is 43.8 μC. The charge associated with an oxide monolayer on palladium metal electrodes is ca. 424 μC cm^{-2}Pd.[116] The active surface area of palladium on the electrode is therefore

$$43.8\ \mu C/424\ \mu cm^{-2}=0.103\ cm^2$$

For NPs with an average diameter of 3.60 nm, if the NPs are assumed to be isolated from each other, the number of NPs on the electrode surface is therefore 2.5 x 10^{11}, with a surface coverage of 3.6 x 10^{12} NPs/cm^2. If the number of Pd atoms per particle is 1662, there are 5.9 x 10^{15} Pd atoms/cm^2, for a total of 4.2 x 10^{14} Pd atoms on

the electrode surface. This is comparable to 4.2 x 10^{15} Pd atoms/cm^2 for 3.1 nm particles synthesized by Takasu and co-workers for vacuum deposited Pd NPs on glassy carbon.[118] Integrating under C2 from Figure 12 gives a charge of 64 $\mu C/cm^2$ Pd. Compared to a charge of 210 $\mu C/cm^2$ Pd for a complete monolayer of hydrogen on Pd[75] this value corresponds to 30% of a monolayer. This behavior has been observed in previous studies for Pd deposited on a gold substrate in basic solution, in which a 36% surface coverage was observed.[76] While the exact cause of a cathodic adsorption charge for hydrogen adsorption in base is not clear, it possibly arises from contamination in the solution, similar to crystal violet, which completely blocks adsorption.[72,73] Lasia and co-workers have speculated that possible contaminants could include carbonates, as well as silicates from dissolved glass, which is very likely in this case.[75]

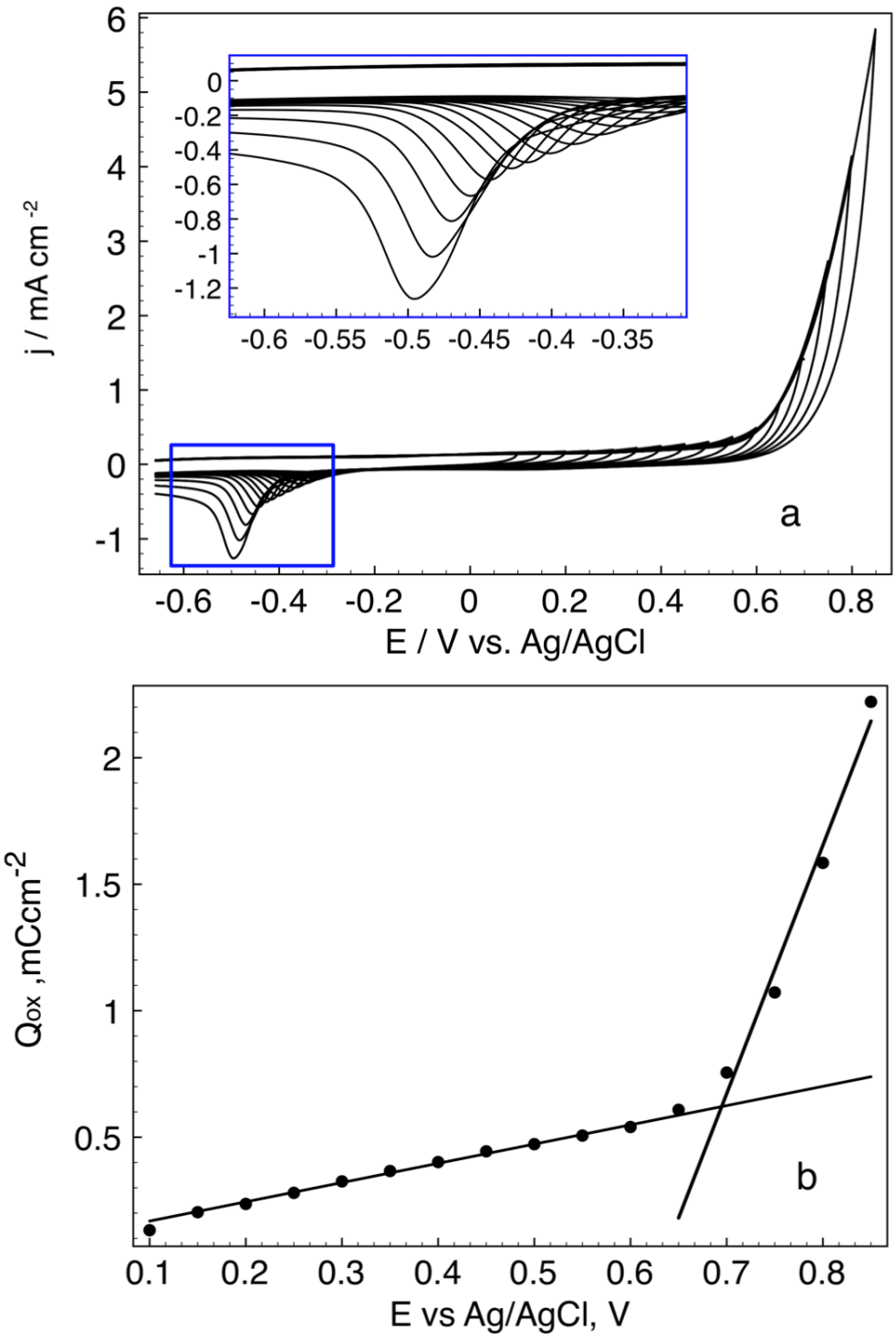

Figure. 13. (a) CV of NP modified GCE in oxide region with anodic oxide limit increased from 0.1 V to 0.85 V in 50 mV increments, inset: magnified view of oxide reduction region, . (b) Plot of oxide reduction charge vs. anodic potential limit. Scan rate = 50 mV/s

Dependence of Hydrogen Loading on Minimum Potential

The atomic ratio of absorbed hydrogen to palladium (H_{abs}:Pd) was determined as a function of the cathodic potential limit. Integration of the anodic peaks A3 and A2/A2' gives the total charge for oxidation of absorbed $\alpha + \beta$ phase, and adsorbed hydrogen, respectively. To calculate the charge contribution from only the absorbed hydrogen in the α and β phases the charge due to hydrogen adsorption, determined by integrating peak C2 was subtracted from this total. The H:Pd ratio was obtained by dividing number of absorbed hydrogen atoms determined from this charge by the number of palladium atoms on the electrode surface determined above. Figure 14 shows the calculated H:Pd ratio as a function of the cathodic scanning potential which is analogous to pressure in hydrogen gas absorption in hydrogen. The shape of the plot resembles similar data given by Rose and co-workers who investigated the effect of potential on the H:Pd ratio in carbon-supported palladium nanoparticles in acid.[70,71] Their studies interestingly show an overcharge, or hyperstoichiometric H:Pd ratio which was attributed to re-oxidation of molecular hydrogen trapped in the electrode. Gabrielli and co-workers and Bartlett and co-workers found a similar trend for hydrogen absorbed in palladium thin films.[119,68] These studies all show several distinct regions of hydrogen content with respect to potential. At more positive potentials, the H:Pd ratio is low, attributed to α-phase formation, in this case from ca. -1 V to -1.1 V. As the potential is made further negative (ca. -1.1 to ca -1.3 V), there is a more rapid increase in the hydrogen content indicating the onset of the β-phase and corresponding to the mixed α and β phase region. At more negative potentials, the system exists solely in the β phase until a maximum value for

H:Pd of ca. 0.7 is reached. At more negative potentials, voltammetry shows significant contribution to the anodic charge by oxidation of evolved hydrogen. The higher fraction of surface vs. interior atoms for nanostructured Pd allows for better distinction of the adsorption and absorption of hydrogen as opposed to bulk systems in which the absorption process dominates the voltammetry.[108] The unique characteristics of the Pd NPs prepared here give better differentiation of the various processes, which allows for a better quantitation of the H/Pd ratio. In the present case, the limiting ratio is observed to be 0.65 – 0.7, in excellent agreement with previous measurements.[67,69,74]

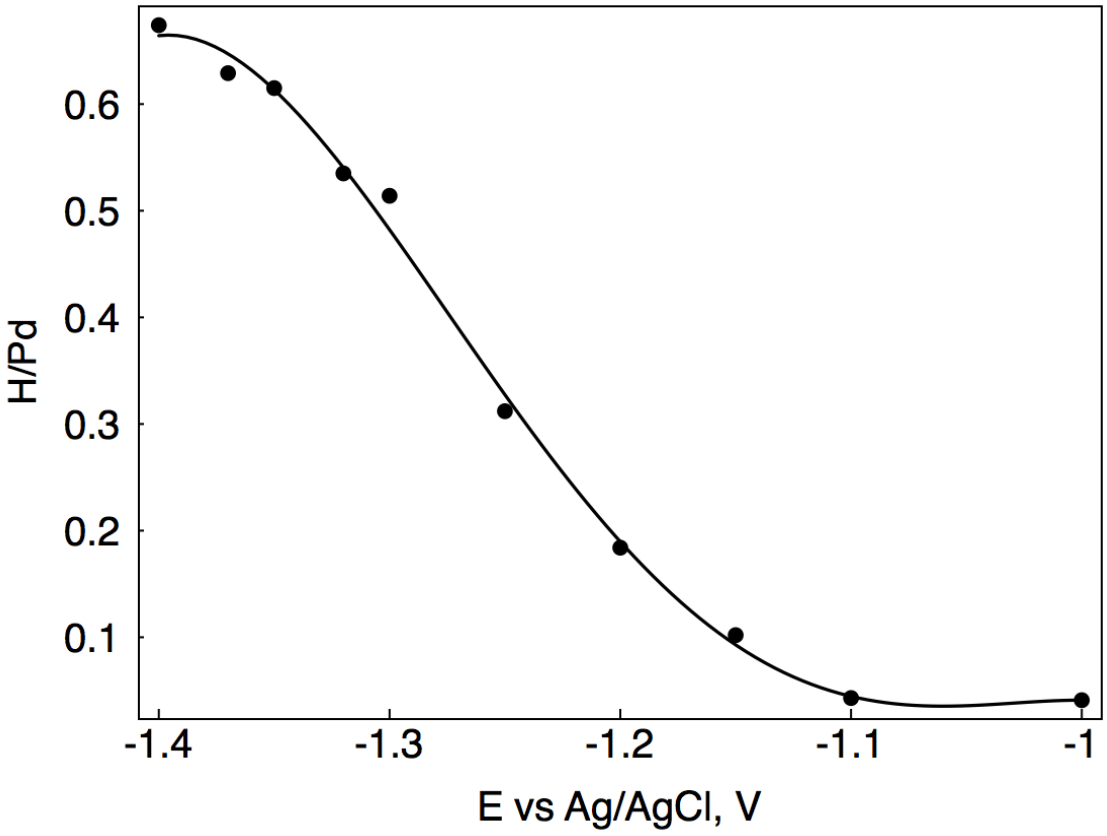

Figure.14. Plot of the H:Pd ratio as a function of the cathodic potential limit for the PdNP modified GCE. Scan rate = 100 mV/s.

Conclusion: This thesis describes the synthesis of stable, water-soluble adenosine-5'-triphosphate capped palladium nanoparticles. UV-Vis analysis is consistent with the calculated spectrum for Pd NPs.[32] The particle size could be varied from 2.5 nm to 3.6 nm with good size dispersity based on TEM characterization by varying the molar ratios of the Pd salt, the capping ligand and the reducing agent. XRD studies confirm the fcc structure of the Pd, as well as an expansion of the lattice possibly due to surface oxide.[92,93] SEM/EDS suggest that ATP has a high surface coverage with a perpendicular orientation relative to the NP surface, similar to binding on gold[97] and silver[99] surfaces. The Pd NPs were firmly attached to a glassy carbon working electrode via a novel deposition method by cycling the GCE in a NP solution with K_2SO_4 supporting electrolyte. Electrochemical hydrogen insertion in the NPs was investigated in base by cyclic voltammetry by varying the scan rate in the region of hydrogen adsorption. Two peaks were (A2 and A2') observed in the anodic sweep, which were attributed to two different types of adsorbed hydrogen, as had been observed in previous studies.[74,77] Both peaks shifted to more positive potentials as the scan rate increased, indicative of an irreversible process. The effect of the scan rate was also investigated in the region of hydrogen absorption. The absorption (C3) and oxidation (A3) peaks became more separated as the scan rate was increased due to the migration of the α-β phase boundary through the NP which involved a change in lattice parameter. The total Pd surface area, and correspondingly the NP density on the electrode were determined by cycling into the Pd oxide formation region and determining the charge associated with the formation of an oxide monolayer. The total Pd surface area in this case was found to be 0.103 cm^2 with a NP density of 3.6×10^{12} NPs/cm^2. Based on the known surface area and the

integrated charge for the hydrogen adsorption peak (C2) it was determined that 30% of a monolayer of hydrogen was adsorbed on the Pd surface, which had been seen in previous Pd hydrogen studies in base[75] while studies in acid show a complete hydrogen monolayer. Analyzing the hydrogen content in the Pd NPs as a function of the negative potential limit has yielded results in good agreement with electrochemical studies for the PdH system in nanoparticle[70,74,118] and thin film palladium electrodes.[68,69]

References

(1) Roduner, E.: Size matters: why nanomaterials are different. *Chem Soc Rev* **2006**, *35*, 583-592.

(2) Angappane, S.; Park, J.; Jang, Y.; Hyeon, T.; Park, J.-G.: Magnetic Pd nanoparticles: effects of surface atoms. *J Phys-Condens Mat* **2008**, *20*, 295209.

(3) Coronado, E.; Ribera, A.; Garcia-Martinez, J.; Linares, N.; Liz-Marzan, L. M.: Synthesis, Characterization and Magnetism of Monodispersed Water Soluble Palladium Nanoparticles. *J Mater Chem* **2008**, *18*, 5682-5688.

(4) Mulvaney, P.: Surface plasmon spectroscopy of nanosized metal particles. *Langmuir* **1996**, *12*, 788-800.

(5) Hayden, B. E.; Pletcher, D.; Suchsland, J.-P.; Williams, L. J.: The influence of support and particle size on the platinum catalysed oxygen reduction reaction. *Phys Chem Chem Phys* **2009**, *11*, 9141-9148.

(6) Wendt, H.; Spinace, E. V.; Neto, A. O.; Linardi, M.: Electrocatalysis and electrocatalysts for low temperature fuel cells: Fundamentals, state of the art, research and development. *Quim Nova* **2005**, *28*, 1066-1075.

(7) Centi, G.; Perathoner, S.: The Role of Nanostructure in Improving the Performance of Electrodes for Energy Storage and Conversion. *Eur J Inorg Chem* **2009**, 3851-3878.

(8) El-Deab, M.; Ohsaka, T.: An extraordinary electrocatalytic reduction of oxygen on gold nanoparticles-electrodeposited gold electrodes. *Electrochem Commun* **2002**, *4*, 288-292.

(9) El-Deab, M.; Okajima, T.; Ohsaka, T.: Electrochemical reduction of oxygen on gold nanoparticle-electrodeposited glassy carbon electrodes. *J Electrochem Soc* **2003**, *150*, A851-A857.

(10) Raj, C.; Abdelrahman, A.; Ohsaka, T.: Gold nanoparticle-assisted electroreduction of oxygen. *Electrochem Commun* **2005**, *7*, 888-893.

(11) Erikson, H.; Juermann, G.; Sarapuu, A.; Potter, R. J.; Tammeveski, K.: Electroreduction of oxygen on carbon-supported gold catalysts. *Electrochim Acta* **2009**, *54*, 7483-7489.

(12) Guo, J. S.; Hsu, A.; Chu, D.; Chen, R. R.: Improving Oxygen Reduction Reaction Activities on Carbon-Supported Ag Nanoparticles in Alkaline Solutions. *Journal of Physical Chemistry* **2010**, *114*.

(13) Jiang, L.; Hsu, A.; Chu, D.; Chen, R.: Size-Dependent Activity of Palladium Nanoparticles for Oxygen Electroreduction in Alkaline Solutions. *J Electrochem Soc* **2009**, *156*, B643-B649.

(14) Xia, Y.; Xiong, Y.; Lim, B.; Skrabalak, S. E.: Shape-Controlled Synthesis of Metal Nanocrystals: Simple Chemistry Meets Complex Physics? *Angew. Chem. Int. Ed.* **2009**, *48*, 60-103.

(15) Lim, B.; Xiong, Y.; Xia, Y.: A water-based synthesis of octahedral, decahedral, and icosahedral Pd nanocrystals. *Angew Chem Int Edit* **2007**, *46*, 9279-9282.

(16) LaMer, V. K.; Dinegar, R. H.: Theory, Production and Mechanism of Formation of Monodispersed Hydrosols. *J. Am. Chem. Soc* **1950**, *72*, 4847-4854.

(17) Kwon, S. G.; Hyeon, T.: Colloidal Chemical Synthesis and Formation Kinetics of Uniformly Sized Nanocrystals of Metals, Oxides, and Chalcogenides. *Accounts Chem Res* **2008**, *41*, 1696-1709.

(18) Murray, C. B.; J., N. D.; Bawendi, M. G.: Synthesis and Characterization of Nearly Monodisperse CdE
(E = S, Se, Te) Semiconductor Nanocrystallites. *J Am Chem Soc* **1993**, *115*, 8706-8715.

(19) Richards, V. N.; Rath, N. P.; Buhro, W. E.: Pathway from a Molecular Precursor to Silver Nanoparticles: The Prominent Role of Aggregative Growth. *Chem Mater* **2010**, *22*, 3556-3567.

(20) Takesue, M.; Tomura, T.; Yamada, M.; Hata, K.; Kuwamoto, S.; Yonezawa, T.: Size of Elementary Clusters and Process Period in Silver Nanoparticle Formation. *J Am Chem Soc* **2011**, *133*, 14164-14167.

(21) Brust, M.; Walker, M.; Bethell, D.; Schiffrin, D.; Whyman, R.: Synthesis of Thiol-derivatised Gold Nanoparticles in a Two-phase Liquid-Liquid System. *J Chem Soc Chem Comm* **1994**, 801-802.

(22) Chaki, N.; Sharma, J.; Mandle, A.; Mulla, I.; Pasricha, R.; Vijayamohanan, K.: Size dependent redox behavior of monolayer protected silver nanoparticles (2-7 nm) in aqueous medium. *Phys Chem Chem Phys* **2004**, *6*, 1304-1309.

(23) Zamborini, F.; Gross, S.; Murray, R.: Synthesis, characterization, reactivity, and electrochemistry of palladium monolayer protected clusters. *Langmuir* **2001**, *17*, 481-488.

(24) Chen, S.; Huang, K.; Stearns, J.: Alkanethiolate-protected palladium nanoparticles. *Chem Mater* **2000**, *12*, 540-547.

(25) Li, F.; Ciani, I.; Bertoncello, P.; Unwin, P. R.; Zhao, J.; Bradbury, C. R.; Fermin, D. J.: Scanning electrochemical microscopy of redox-mediated hydrogen

evolution catalyzed by two-dimensional assemblies of palladium nanoparticles. *J Phys Chem C* **2008**, *112*, 9686-9694.

(26) Henglein, A.: Colloidal palladium nanoparticles: Reduction of Pd(II) by H-2; PdcoreAushellAgshell particles. *J Phys Chem B* **2000**, *104*, 6683-6685.

(27) Ivanova, O. S.; Zamborini, F. P.: Size-Dependent Electrochemical Oxidation of Silver Nanoparticles. *J Am Chem Soc* **2010**, *132*, 70-+.

(28) Papp, S.; Dékány, I.: Nucleation and growth of palladium nanoparticles stabilized by polymers and layer silicates. *Colloid Polym Sci* **2006**, *284*, 1049-1056.

(29) Lee, Y. W.; Kim, N. H.; Lee, K. Y.; Kwon, K.; Kim, M.; Han, S. W.: Synthesis and characterization of flower-shaped porous Au-Pd alloy nanoparticles. *J Phys Chem C* **2008**, *112*, 6717-6722.

(30) Evangelisti, C.; Panziera, N.; D'alessio, A.; Bertinetti, L.; Botavina, M.; Vitulli, G.: New monodispersed palladium nanoparticles stabilized by poly-(N-vinyl-2-pyrrolidone): Preparation, structural study and catalytic properties. *Journal of Catalysis* **2010**, *272*, 246-252.

(31) Li, D.; Komarneni, S.: Nanoparticles of Pd: Synthesis by Microwave-Solvothermal Method and Optical Properties. *J Nanosci Nanotechno* **2008**, *8*, 3930-3935.

(32) Creighton, J. A.; Eadon, D. G.: Ultraviolet-Visible Absorption Spectra of the Colloidal Metallic Elements. *J Chem Soc Faraday T* **1991**, *87*, 3881-3891.

(33) Patterson, A.: The Scherrer formula for x-ray particle size determination. *Phys Rev* **1939**, *56*, 978-982.

(34) Ung, T.; GIERSIG, M.; Dunstan, D.; MULVANEY, P.: Spectroelectrochemistry of colloidal silver. *Langmuir* **1997**, *13*, 1773-1782.

(35) Underwood, S.; Mulvaney, P.: Effect of the Solution Refractive Index on the Color of Gold Colloids. *Langmuir* **1994**, *10*, 3427-3430.

(36) Zhao, W.; Gonzaga, F.; Li, Y.; Brook, M. A.: Highly stabilized nucleotide-capped small gold nanoparticles with tunable size. *Adv Mater* **2007**, *19*, 1766-+.

(37) Jiang, C.; Markutsya, S.; Tsukruk, V.: Collective and individual plasmon resonances in nanoparticle films obtained by spin-assisted layer-by-layer assembly. *Langmuir* **2004**, *20*, 882-890.

(38) Murray, R. W.: Nanoelectrochemistry: Metal nanoparticles, nanoelectrodes, and nanopores. *Chem Rev* **2008**, *108*, 2688-2720.

(39) Branham, M. R.; Douglas, A. D.; Mills, A. J.; Tracy, J. B.; White, P. S.; Murray, R. W.: Arylthiolate-protected silver quantum dots. *Langmuir* **2006**, *22*, 11376-11383.

(40) Chen, S.; Huang, K.: Electrochemical studies of water-soluble palladium nanoparticles. *J Clust Sci* **2000**, *11*, 405-422.

(41) Kim, S.; Park, J.; Jang, Y.; Chung, Y.; Hwang, S.; Hyeon, T.; Kim, Y.: Synthesis of monodisperse palladium nanoparticles. *Nano Lett* **2003**, *3*, 1289-1291.

(42) Ariga, K.; Hill, J. P.; Ji, Q.: Layer-by-layer assembly as a versatile bottom-up nanofabrication technique for exploratory research and realistic application. *Phys Chem Chem Phys* **2007**, *9*, 2319-2340.

(43) Srivastava, S.; Kotov, N. A.: Composite Layer-by-Layer (LBL) Assembly with Inorganic Nanoparticles and Nanowires. *Accounts Chem Res* **2008**, *41*, 1831-1841.

(44) Cho, J.; Caruso, F.: Investigation of the interactions between ligand-stabilized gold nanoparticles and polyelectrolyte multilayer films. *Chem Mater* **2005**, *17*, 4547-4553.

(45) Jiang, S.; Li, L.; Liu, Z.; Pan, M.; Tang, H.: Self-assembly of PDDA-Pt nanoparticle/nafion membranes for direct methanol fuel cells. *Electrochem Solid St* **2005**, *8*, A574-A576.

(46) Yamada, M.; Nishihara, H.: Electrochemical deposition of metal nanoparticles functionalized with multiple redox molecules. *Cr Chim* **2003**, *6*, 919-934.

(47) Cao, D.; Sun, L.; Wang, G.; Lv, Y.; Zhang, M.: Kinetics of hydrogen peroxide electroreduction on Pd nanoparticles in acidic medium. *J Electroanal Chem* **2008**, *621*, 31-37.

(48) Grigoriev, S. A.; Lyutikova, E. K.; Martemianov, S.; Fateev, V. N.: On the possibility of replacement of Pt by Pd in a hydrogen electrode of PEM fuel cells. *Int J Hydrogen Energ* **2007**, *32*, 4438-4442.

(49) Hu, F.; Chen, C.; Wang, Z.; Wei, G.; Shen, P. K.: Mechanistic study of ethanol oxidation on Pd-NiO/C electrocatalyst. *Electrochim Acta* **2006**, *52*, 1087-1091.

(50) Xu, C.; Shen, P. k.; Liu, Y.: Ethanol electrooxidation on Pt/C and Pd/C catalysts promoted with oxide. *J Power Sources* **2007**, *164*, 527-531.

(51) Shen, P.; Xu, C.: Alcohol oxidation on nanocrystalline oxide Pd/C promoted electrocatalysts. *Electrochem Commun* **2006**, *8*, 184-188.

(52) Lewis, F. A.: *The Palladium Hydrogen System*; Academic Press Inc. (London) Ltd: London, 1967.

(53) Batchelor-McAuley, C.; Banks, C.; Simm, A.; Jones, T.; Compton, R.: Nano-electrochemical detection of hydrogen or protons using palladium nanoparticles: Distinguishing surface and bulk hydrogen. *Chemphyschem* **2006**, *7*, 1081-1085.

(54) Mclennan, K.; Gray, E.; Dobson, J.: Deuterium occupation of tetrahedral sites in palladium. *Phys. Rev. B* **2008**, *78*, 014104.

(55) Carino, E. V.; Knecht, M. R.; Crooks, R. M.: Quantitative Analysis of the Stability of Pd Dendrimer-Encapsulated Nanoparticles. *Langmuir* **2009**, *25*, 10279-10284.

(56) Crooks, R.; Zhao, M.; Sun, L.; Chechik, V.; Yeung, L.: Dendrimer-encapsulated metal nanoparticles: Synthesis, characterization, and applications to catalysis. *Accounts Chem Res* **2001**, *34*, 181-190.

(57) Kundu, S.; Wang, K.; Lau, S.; Liang, H.: Photochemical synthesis of shape-selective palladium nanocubes in aqueous solution. *J Nanopart Res* **2010**, *12*, 2799-2811.

(58) FLANAGAN, T.; OATES, W.: THE PALLADIUM-HYDROGEN SYSTEM. *Annu Rev Mater Sci* **1991**, *21*, 269-304.

(59) Yamauchi, M.; Ikeda, R.; Kitagawa, H.; Takata, M.: Nanosize effects on hydrogen storage in palladium. *J Phys Chem C* **2008**, *112*, 3294-3299.

(60) Zlotea, C.; Cuevas, F.; Paul-Boncour, V.; Leroy, E.; Dibandjo, P.; Gadiou, R.; Vix-Guterl, C.; Latroche, M.: Size-Dependent Hydrogen Sorption in Ultrasmall Pd Clusters Embedded in a Mesoporous Carbon Template. *J Am Chem Soc* **2010**, *132*, 7720-7729.

(61) Langhammer, C.; Zhdanov, V. P.; Zorić, I.; Kasemo, B.: Size-Dependent Kinetics of Hydriding and Dehydriding of Pd Nanoparticles. *Phys. Rev. Lett.* **2010**, *104*, 135502.

(62) Vogel, W.; He, W.; Huang, Q.-H.; Zou, Z.; Zhang, X.-G.; Yang, H.: Palladium nanoparticles ``breathe'' hydrogen; a surgical view with X-ray diffraction. *Int J Hydrogen Energ* **2010**, *35*, 8609-8620.

(63) Narehood, D. G.; Kishore, S.; Goto, H.; Adair, J. H.; Nelson, J. A.; Gutiérrez, H. R.; Eklund, P. C.: X-ray diffraction and H-storage in ultra-small palladium particles. *Int J Hydrogen Energ* **2009**, *34*, 952-960.

(64) Rather, S.-u.; Zacharia, R.; Hwang, S. W.; Naik, M.-u.; Nahm, K. S.: Hyperstoichiometric hydrogen storage in monodispersed palladium nanoparticles. *Chem Phys Lett* **2007**, *438*, 78-84.

(65) Delogu, F.: Smooth Size Effects in Pd and PdHx Nanoparticles. *J Phys Chem C* **2010**, *114*, 18085-18090.

(66) Breiter, M.: Dissolution and Adsorption of Hydrogen at Smooth Pd Wires at Potentials of Alpha Phase in Sulfuric Acid Solution. *J Electroanal Chem* **1977**, *81*, 275-284.

(67) Czerwinski, A.; Marassi, R.; Zamponi, S.: The Absorption of hydrogen and deuterium in thin palladium electrodes. *J Electroanal Chem* **1991**, *316*, 211-221.

(68) Bartlett, P.; Gollas, B.; Guerin, S.; Marwan, J.: The preparation and characterisation of H-1-e palladium films with a regular hexagonal nanostructure formed by electrochemical deposition from lyotropic liquid crystalline phases. *Phys Chem Chem Phys* **2002**, *4*, 3835-3842.

(69) Gabrielli, C.; Grand, P.; Lasia, A.; Perrot, H.: Investigation of hydrogen adsorption and absorption in palladium thin films - II. Cyclic voltammetry. *J Electrochem Soc* **2004**, *151*, A1937-A1942.

(70) Rose, A.; Maniguet, S.; Mathew, R.; Slater, C.; Yao, J.; Russell, A.: Hydride phase formation in carbon supported palladium nanoparticle electrodes investigated using in situ EXAFS and XRD. *Phys Chem Chem Phys* **2003**, *5*, 3220-3225.

(71) Rose, A.; South, O.; Harvey, I.; Diaz-Moreno, S.; Owen, J.; Russell, A.: In situ time resolved studies of hydride and deuteride formation in Pd/C electrodes via energy dispersive X-ray absorption spectroscopy. *Phys Chem Chem Phys* **2005**, *7*, 366-372.

(72) Bartlett, P.; Marwan, J.: The effect of surface species on the rate of H sorption into nanostructured Pd. *Phys Chem Chem Phys* **2004**, *6*, 2895-2898.

(73) Birry, L.; Lasia, A.: Effect of crystal violet on the kinetics of H sorption into Pd. *Electrochim Acta* **2006**, *51*, 3356-3364.

(74) Tateishi, N.; K, Y.; K, N.; Y, T.: Hydrogen Electrode Reaction on Electrodes of Glassy Carbon-Supported ultrafine Pd Particles in Alkaline Media. *Electrochim Acta* **1992**, *37*, 2427-2432.

(75) Martin, M. H.; Lasia, A.: Study of the hydrogen absorption in Pd in alkaline solution. *Electrochim Acta* **2008**, *53*, 6317-6322.

(76) Martin, M. H.; Lasia, A.: Hydrogen sorption in Pd monolayers in alkaline solution. *Electrochim Acta* **2009**, *54*, 5292-5299.

(77) Denuault, G.; Milhano, C.; Pletcher, D.: Mesoporous palladium - the surface electrochemistry of palladium in aqueous sodium hydroxide and the cathodic reduction of nitrite. *Phys Chem Chem Phys* **2005**, *7*, 3545-3551.

(78) Nemamcha, A.; Rehspringer, J.; Khatmi, D.: Synthesis of palladium nanoparticles by sonochemical reduction of palladium(II) nitrate in aqueous solution. *J Phys Chem B* **2006**, *110*, 383-387.

(79) Xiong, Y.; Wiley, B.; Chen, J.; Li, Z.; Yin, Y.; Xia, Y.: Corrosion-based synthesis of single-crystal Pd nanoboxes and nanocages and their surface plasmon properties. *Angew Chem Int Edit* **2005**, *44*, 7913-7917.

(80) Scott, R.; Ye, H.; Henriquez, R.; Crooks, R.: Synthesis, characterization, and stability of dendrimer-encapsulated palladium nanoparticles. *Chem Mater* **2003**, *15*, 3873-3878.

(81) Tateishi, N.; Yahikozawa, K.; Nishimura, K.; Takasu, Y.: Hydrogen Electrode-Reaction On Electrodes Of Glassy Carbon-Supported Ultrafine Pd Particles In Alkaline Media. *Electrochim Acta* **1992**, *37*, 2427-2432.

(82) Green, M.; Taylor, R.; Wakefield, G.: The synthesis of luminescent adenosine triphosphate passivated cadmium sulfide nanoparticles. *J Mater Chem* **2003**, *13*, 1859-1861.

(83) Chemseddine, A.; Weller, H.: Highly Monodisperse Quantum-Sized CdS particles by Size-Selective Precipitation. *Ber Bunsen Phys Chem* **1993**, *97*, 636-637.

(84) Hu, Y.; Zhang, H.; Wu, P.; Zhang, H.; Zhou, B.; Cai, C.: Bimetallic Pt–Au nanocatalysts electrochemically deposited on graphene and their electrocatalytic characteristics towards oxygen reduction and methanol oxidation. *Phys Chem Chem Phys* **2011**, *13*, 4083.

(85) Peral, F.; Gallego, E.: The self-organization of adenosine 5 '-triphosphate and adenosine 5 '-diphosphate in aqueous solution as determined from ultraviolet hypochromic effects. *Biophys Chem* **2000**, *85*, 79-92.

(86) Van Hyning, D.; Klemperer, W.; Zukoski, C.: Silver nanoparticle formation: Predictions and verification of the aggregative growth model. *Langmuir* **2001**, *17*, 3128-3135.

(87) Van Hyning, D.; Zukoski, C.: Formation mechanisms and aggregation behavior of borohydride reduced silver particles. *Langmuir* **1998**, *14*, 7034-7046.

(88) International Centre for Diffraction Data. **2010**.

(89) Qi, W.; Wang, M.; Su, Y.: Size effect on the lattice parameters of nanoparticles. *J Mater Sci Lett* **2002**, *21*, 877-878.

(90) Lamber, R.; Wetjen, S.; Jaeger, N.: Size Dependence Of The Lattice-Parameter Of Small Palladium Particles. *Phys. Rev. B* **1995**, *51*, 10968-10971.

(91) Khanuja, M.; Mehta, B. R.; Agar, P.; Kulriya, P. K.; Avasthi, D. K.: Hydrogen induced lattice expansion and crystallinity degradation in palladium nanoparticles: Effect of hydrogen concentration, pressure, and temperature. *J. Appl. Phys.* **2009**, *106*, 093515.

(92) Ingham, B.; Toney, M. F.; Hendy, S. C.; Cox, T.; Fong, D. D.; Eastman, J. A.; Fuoss, P. H.; Stevens, K. J.; Lassesson, A.; Brown, S. A.; Ryan, M. P.: Particle size effect of hydrogen-induced lattice expansion of palladium nanoclusters. *Phys. Rev. B* **2008**, *78*, 245408.

(93) Oh, C.; Hong, K. S.; Lee, S.; Park, C.-h.; Yu, I.: Catalytic oxidation of hydrogen at nanocrystalline palladium surfaces. *J Phys-Condens Mat* **2006**, *18*, 3335-3341.

(94) Akita, T.; Hiroki, T.; Tanaka, S.; Kojima, T.; Kohyama, M.; Iwase, A.; Hori, F.: Analytical TEM observation of Au-Pd nanoparticles prepared by sonochemical method. *Catal Today* **2008**, *131*, 90-97.

(95) Lu, J.; Stair, P. C.: Nano/Subnanometer Pd Nanoparticles on Oxide Supports Synthesized by AB-type and Low-Temperature ABC-type Atomic Layer Deposition: Growth and Morphology †. *Langmuir* **2010**, *26*, 16486-16495.

(96) Xiong, Y.; Xia, Y.: Shape-controlled synthesis of metal nanostructures: The case of palladium. *Adv Mater* **2007**, *19*, 3385-3391.

(97) Prado, C.; Prieto, F.; Rueda, M.; Feliu, J.; Aldaz, A.: Adenine adsorption on Au(111) and Au(100) electrodes: Characterisation, surface reconstruction effects and thermodynamic study. *Electrochim Acta* **2007**, *52*, 3168-3180.

(98) Kundu, J.; Neumann, O.; Janesko, B. G.; Zhang, D.; Lal, S.; Barhoumi, A.; Scuseria, G. E.; Halas, N. J.: Adenine- and Adenosine Monophosphate (AMP)-Gold Binding Interactions Studied by Surface-Enhanced Raman and Infrared Spectroscopies. *J Phys Chem C* **2009**, *113*, 14390-14397.

(99) Giese, B.; McNaughton, D.: Surface-enhanced Raman spectroscopic and density functional theory study of adenine adsorption to silver surfaces. *J Phys Chem B* **2002**, *106*, 101-112.

(100) Burke, L. D.; Casey, J. K.: An Examination of the Electrochemical Bahavior of Palladium in Base. *J Electrochem Soc* **1993**, *140*, 1292-1298.

(101) Birss, V.; Beck, V.; Zhang, A.; Vanysek, P.: Properties of thin, hydrous Pd oxide films. *J Electroanal Chem* **1997**, *429*, 175-184.

(102) Singh, P.; Parent, K. L.; Buttry, D. A.: Electrochemical Solid-State Phase Transformations of Silver Nanoparticles. *J Am Chem Soc* **2012**, *134*, 5610-5617.

(103) Campesi, R.; Cuevas, F.; Gadiou, R.; Leroy, E.; Hirscher, M.; Vix-Guterl, C.; Latroche, M.: Hydrogen storage properties of Pd nanoparticle/carbon template composites. *Carbon* **2008**, *46*, 206-214.

(104) Mushrif, S. H.; Rey, A. D.; Peslherbe, G. H.: Energetics and dynamics of hydrogen adsorption, desorption and migration on a carbon-supported palladium cluster. *J Mater Chem* **2010**, *20*, 10503.

(105) Pattabiraman, R.: Electrochemical investigations on carbon supported palladium catalysts. *Appl Catal A-Gen* **1997**, *153*, 9-20.

(106) Sagade, A. A.; Radha, B.; Kulkarni, G. U.: Intricate nature of Pd nanocrystalâ€“hydrogen interaction investigated using thermolysed Pd hexadecylthiolate films. *Sensors & Actuators: B. Chemical* **2031**, *149*, 345-351.

(107) Bolzan, A.: An interpretation of the different processes involved in the electroreduction of thick palladium oxide films. *J Electroanal Chem* **1997**, *437*, 199-208.

(108) Bolzan, A.: Phenomenological aspects related to the electrochemical bahaviour of smooth palladium electrodes in alkaline solutions. *J Electroanal Chem* **1995**, *380*, 127-138.

(109) Conway, B.: Electrochemical Oxide Film Formation At Noble-Metals As A Surface-Chemical Process. *Prog Surf Sci* **1995**, *49*, 331-452.

(110) Zhang, W.; Zhang, X.; Zhao, X.: Voltammograms of thin layer Pd vertical bar H(D) electrodes in the coexistence of alpha and beta phases. *J Electroanal Chem* **1998**, *458*, 107-112.

(111) Breger, V.; Gileadi, E.: Adsorption and Absorption of Hydrogen in Palladium. *Electrochim Acta* **1971**, *16*, 177-&.

(112) Millet, P.: Thermodynamic paths in the two-phases domain of the PdH system and a method for kinetic analysis. *Electrochem Commun* **2005**, *7*, 40-44.

(113) Chierchie, T.; Mayer, C.: Voltammetric Study of the Underpotential Deposition of Copper on Polycrystalline and Single-Crystal Palladium Surfaces. *Electrochim Acta* **1988**, *33*, 341-345.

(114) Lenz, P.; Solomun, T.: Underpotential Deposition of Copper on Pd (1 0 0) - An Electron Spectroscopy Study. *J Electroanal Chem* **1993**, *353*, 131-145.

(115) Fang, L.-l.; Tao, Q.; Li, M.-f.; Liao, L.-w.; Chen, D.; Chen, Y.-x.: Determination of the Real Surface Area of Palladium Electrode. *Chinese J Chem Phys* **2010**, *23*, 543-548.

(116) Rand, D.; Woods, R.: Determination of Real Surface Area of Palladium Electrodes. *Anal Chem* **1975**, *47*, 1481-1483.

(117) Correia, A.; Mascaro, L.; Machado, S.; Avaca, L.: Active surface area determination of Pd-Si alloys by H-adsorption. *Electrochim Acta* **1997**, *42*, 493-495.

(118) Tateishi, N.; Yahikozawa, K.; Nishimura, K.; Suzuki, M.; Iwanaga, Y.; Watanabe, M.; Enami, E.; Matsuda, Y.; Takasu, Y.: Electrochemical Properties Of Ultra-Fine Palladium Particles For Adsorption And Absorption Of Hydrogen In An Aqueous Hclo4 Solution. Electrochim Acta 1991, 36, 1235-1240.

(119) Gabrielli, C.; Grand, P.; Lasia, A.; Perrot, H.: Study of the hydrogen/palladium system by fast quartz microbalance techniques. *Electrochim Acta* **2002**, *47*, 2199-2207.

55